Single top quark production and decay in the t channel at next-to-leading order at the LHC

Reinhard Schwienhorst, C.-P. Yuan, Charles Mueller, and Qing-Hong Cao

Phys. Rev. D **83**, 034019 — Published 16 February 2011

DOI: 10.1103/PhysRevD.83.034019

Single top quark production and decay in the t-channel at next-to-leading order at the LHC

Reinhard Schwienhorst,* C.-P. Yuan,† and Charles Mueller‡

Department of Physics & Astronomy,

Michigan State University, East Lansing, MI 48824, USA

Qing-Hong Cao§

HEP Division, Argonne National Laboratory, Argonne, IL 60439, U.S.A and

Enrico Fermi Institute, University of Chicago, Chicago, Illinois 60637, U.S.A.

Abstract

We present a study of single top and single antitop quark production in the t-channel mode at the LHC pp collider at 7 TeV, 10 TeV and 14 TeV, including next-to-leading order QCD corrections to the production and decay of the top quark. We discuss the effects of different $O(\alpha_s)$ contributions on the inclusive cross section and important kinematic distributions, after imposing the relevant cuts to select t-channel single top quark events.

*Electronic address: schwier@pa.msu.edu

†Electronic address: yuan@pa.msu.edu

‡Electronic address: muell149@msu.edu

§Electronic address: caoq@hep.anl.gov

I. INTRODUCTION

The top quark and its electroweak interaction are important within the Standard Model and provide a window to physics beyond the standard model. In particular the production of single top quarks through electroweak interactions is a sensitive process at hadron colliders that is being studied at both the Tevatron proton-antiproton collider and the Large Hadron Collider (LHC) proton-proton collider. Electroweak single top quark production proceeds through the s-channel decay of a virtual W ($q\bar{q}' \to W^* \to t\bar{b}$), the t-channel exchange of a virtual W ($bq \to tq'$ and $b\bar{q}' \to t\bar{q}$, shown in Fig. 1), and the associated production of a top quark and a W boson ($bg \to tW^-$). The single top cross section is proportional to the Cabibbo-Kobayashi-Maskawa (CKM) quark mixing matrix element $|V_{tb}|^2$, and the single top cross section measurement provides a direct determination of $|V_{tb}|$ without assumptions about the number of quark generations. A study of spin correlations in single top quark production can be used to test the left-handed nature of the top quark charged-current weak interaction and to look for anomalous top quark couplings [1–3].

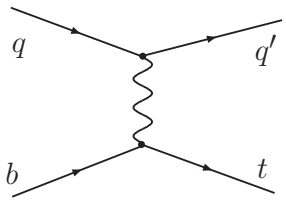

FIG. 1: Representative Feynman diagram for t-channel single top quark production.

The DØ and CDF collaborations at the Fermilab Tevatron proton-antiproton collider have observed single top quark production for the first time [4–6], following the evidence for single top production from DØ [7, 8], confirmed by CDF [9]. The Tevatron measurements combine the s-channel and t-channel signals to maximize the sensitivity to the single top quark signal. The DØ collaboration has also reported a separate measurement of the t-channel cross section [10], independent of the s-channel. These measurements rely heavily on multivariate analysis techniques [8, 11, 12] which require accurate modeling of both the single top signals and the various background processes.

At the LHC, single top quark production will play an important role in searches for new physics, in the single top quark final state and as background in other searches. All three single top processes should be observed at the LHC, where the t-channel has the

largest cross section, followed by associated production and the s-channel. It is important to separate these processes from each other since they have different systematic uncertainties and different sensitivities to new physics [13–16].

The next-to-leading order (NLO) $O(\alpha_s)$ corrections to single top quark production have already been carried out in Refs. [17, 18], which shows an uncertainty on the total cross section of about 5% by varying the factorization and renormalization scales. The differential cross sections for on-shell single top quark production have been calculated [19, 20], and the complete NLO calculations including both the single top quark production and decay have been done independently by several groups [21–28]. For the t-channel process, the NLO corrections have also been calculated for the $2 \to 3$ process $gq \to tq'\overline{b}$ [29, 30], and interference between top quark production and decay have been included [28]. The total cross section has been calculated at NLO including higher order soft gluon corrections [31–33]. Recently, resummation effects on the s- and t-channel single top productions in the framework of soft-collinear-effective-theory have been investigated [34, 35]. In previous studies we presented a detailed phenomenological analysis, focusing on signal cross sections and kinematical distributions, of t-channel single top quark production at the Tevatron [24], and s-channel single top quark production at the LHC [36]. Here we analyze t-channel single top quark production at the LHC proton-proton collider at center of mass (CM) energies of 7 TeV, 10 TeV and 14 TeV. Since the LHC is pp collider, the production cross sections and kinematic distributions are different for $b\bar{t}(j)$ and $t\bar{b}(j)$. We therefore consider the production of a t-quark separately from the production of a $\overline{t}$-quark.

The paper is organized as follows. In Sec. II, we first present the inclusive cross section for single top quark production at the LHC in the t-channel mode. We then investigate its dependence on the top quark mass, renormalization and factorization scales, and parton distribution functions (PDF). In Sec. III, we examine the acceptance of single top quark events for various sets of kinematic cuts. In Sec. IV, we explore the kinematical information in the final state objects. Section V contains our conclusions.

II. INCLUSIVE CROSS SECTION

The LHC will produce large samples of t-channel single top quark events, already in the initial 7 TeV run and even more so in 14 TeV running, and single top quark production

can be studied in detail. The accuracy of the cross section and $|V_{tb}|$ measurements at the Tevatron is limited by the statistical uncertainty of the small single top samples collected and the large backgrounds [4, 5]. The situation will be drastically different at the LHC where systematic uncertainties dominate. In particular the measurement of $|V_{tb}|$ requires accurate theoretical predictions of both the inclusive cross section and kinematic distributions. In this section, we show the inclusive production rates and discuss their dependence on the factorization and renormalization scales as well as the top quark mass.

We present numerical results for the production of single top quark events considering the leptonic decay of the W-boson from the top quark decay at the LHC. We consider three different CM energies for the LHC pp collider: the start-up CM energy of 7 TeV, an intermediate energy of 10 TeV, and the design energy of 14 TeV. Unless otherwise specified, we use the NLO PDF set CTEQ6.6M [37, 38], defined in the $\overline{MS}$ scheme, and the NLO (2-loop) running coupling α_s with $\Lambda_{\overline{MS}}$ provided by the PDFs. For the CTEQ6.6M PDFs, $\Lambda^{(4)}_{\overline{MS}} = 0.326$ GeV for four active quark flavors. The values of the relevant electroweak parameters are: $\alpha = 1/137.0359895$, $G_\mu = 1.16637 \times 10^{-5}\,\mathrm{GeV}^{-2}$, $M_W = 80.40\,\mathrm{GeV}$, $M_Z = 91.1867\,\mathrm{GeV}$, and $\sin^2\theta_W = 0.231$ [39]. The square of the weak gauge coupling is $g^2 = 4\sqrt{2}M_W^2 G_\mu$. We extend our previous Tevatron studies [22–24] to the LHC proton-proton collider, including both top and antitop production. We focus on the electron final state, though our analysis procedure also applies to the muon final state. Including $O(\alpha_s)$ corrections to the decay $W \to \bar{q}q'$, the decay branching ratio of the W boson into leptons is $Br(W \to \ell^+\nu) = 0.108$ [39]. Unless otherwise specified, we will choose the top quark mass to be $m_t = 173\,\mathrm{GeV}$, consistent with the world average [40–42], and the renormalization scale (μ_R) as well as the factorization scale (μ_F) to be equal to the top quark mass.

A. Theoretical cutoff dependence

The NLO QCD differential cross sections are calculated using the one-cutoff phase space slicing (PSS) method [43, 44]. This procedure introduces a theoretical cutoff parameter (s_{min}) in order to isolate soft and collinear singularities associated with real gluon emission sub-processes by partitioning the phase space into soft, collinear and hard regions such that

$$|\mathcal{M}^{\mathrm{r}}|^2 = |\mathcal{M}^{\mathrm{r}}|^2_{\mathrm{soft}} + |\mathcal{M}^{\mathrm{r}}|^2_{\mathrm{collinear}} + |\mathcal{M}^{\mathrm{r}}|^2_{\mathrm{hard}} \ . \tag{1}$$

In the soft and collinear regions the cross section is proportional to the Born-level cross section. Using dimensional regularization, we evaluate the real gluon emission diagrams in n-dimensions under the soft gluon approximation in the soft region and under the collinear approximation in the collinear region, and integrate out the corresponding phase space volume analytically. The resulting divergences are canceled by virtual corrections or absorbed into the perturbative parton distribution functions in the factorization procedure. For our study, we found a cutoff value of $s_{min} = 1\,\mathrm{GeV}^2$ to be appropriate for studying the t-channel single top process. For comparison, we also used a value of $s_{min} = 1\,\mathrm{GeV}^2$ in our Tevatron t-channel study [24], and a value of $s_{min} = 5\,\mathrm{GeV}^2$ in our Tevatron [23] and LHC [36] s-channel studies. A detailed discussion of the phase space slicing method can be found in Ref. [22].

B. Inclusive cross section

The LHC has been designed for a CM energy of 14 TeV, though during the initial start-up of the accelerator the energy is only 7 TeV. Figure 2 shows the dependence of the inclusive cross section on the CM energy.

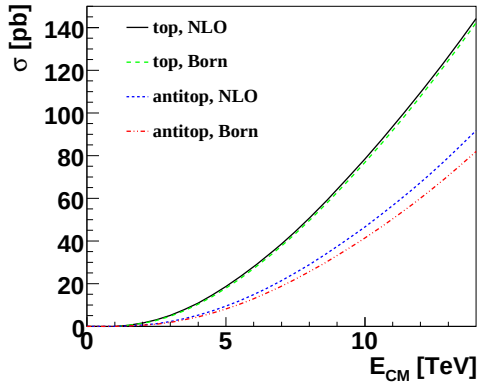

FIG. 2: Inclusive t-channel single top quark cross section at the LHC proton-proton collider as a function of CM energy for a top quark mass of 173 GeV.

At Born-level, the production cross section for top quarks is about 3/2 larger than that for antitop quarks due to the initial state configuration (up quark PDF vs down quark PDF). The difference between top and antitop is smaller at NLO, and the antitop production cross section is larger at NLO compared to Born-level. This is in contrast to the top quark pro-

	Top quark production		Antitop quark production	
	Cross section (pb)	Fraction of NLO (%)	Cross section (pb)	Fraction of NLO (%)
7 TeV CM energy:				
Born-level	38.6	96.6	19.1	87.2
$O(\alpha_s)$ HEAVY	-3.6	-9.0	0.84	3.8
$O(\alpha_s)$ LIGHT	3.9	9.7	1.8	8.0
$O(\alpha_s)$ TDEC	1.1	2.7	0.22	1.0
$O(\alpha_s)$ sum	1.4	3.4	2.8	12.8
NLO	40.0	100	21.9	100
14 TeV CM energy:				
Born-level	146.5	97.2	84.3	87.7
$O(\alpha_s)$ HEAVY	-9.0	-6.0	6.9	7.2
$O(\alpha_s)$ LIGHT	9.0	6.0	3.9	4.1
$O(\alpha_s)$ TDEC	4.2	2.8	1.0	1.0
$O(\alpha_s)$ sum	4.2	2.8	11.8	12.3
NLO	150.7	100	96.1	100

TABLE I: Inclusive t-channel single top production cross section for different sub-processes at the 7 TeV and 14 TeV LHC for a top quark mass of 173 GeV.

duction cross section, which is almost identical between Born-level and NLO. This difference between top and antitop quarks is due to the different b quark and gluon PDF momentum fraction regions.

We group the higher-order QCD corrections into three separate gauge invariant sets according to their origin: corrections from the light quark line (LIGHT), corrections from the heavy quark line (HEAVY), and corrections from the top quark decay (TDEC). If appropriate we further subgroup the HEAVY corrections into those with real gluon emission (HEAVY(g)) and those with emission of a $\bar{b}$-quark (HEAVY($\bar{b}$), also called $2 \to 3$), see also Fig. 6. The explicit diagrams and definitions for these three sets can be found in Ref. [22]. The inclusive cross section as well as the individual $O(\alpha_s)$ contributions are listed in Table I.

The effects of the finite widths of the top quark and W-boson have been included. The

cross section is about twice as large for top quark production compared to antitop because there are two up quarks in the proton and only one down quark. The ratio between top and antitop quark production decreases at NLO due to the heavy quark correction, which has opposite sign for top and antitop quark production. In top quark production, the HEAVY correction is negative, whereas in antitop quark production it is positive. This is a reflection of the different gluon and b quark momentum fractions that the two processes are sensitive to. The TDEC contribution is small compared to the other two.

C. Top quark mass, PDF and renormalization/factorization scale dependence

The inclusive cross section as given in Table I has three uncertainty components. The top quark mass is not known exactly and a change in the mass results in a changing cross section. The t-channel cross section is especially sensitive to the PDFs, in particular of the gluon and the b quark. The renormalization and factorization scales also contribute to the uncertainty of the theoretical prediction. The renormalization scale μ_R is introduced when redefining the bare parameters in terms of the renormalized parameters in the $O(\alpha_s)$ corrections, while the factorization scale μ_F is introduced when absorbing the collinear divergences into parton distribution functions. Therefore, both μ_R and μ_F are unphysical and the final predictions should not depend on them. However, since we work at a fixed order in perturbation theory, we indeed see a dependence of the predicted cross section on μ_R and μ_F, which is formally of higher order. Here, we examine the top quark mass, PDF, and scale dependence of the t-channel inclusive cross section.

Figure 3 shows the top quark mass dependence of the cross section for top and antitop quark production, at Born-level and NLO. Each cross section changes by about $\pm 1.1\%$ when the top quark mass m_t is varied by its current uncertainty of 1.1 GeV around 173 GeV [42]. The uncertainty is larger for lower CM energies, as show in Table II.

The usual practice for estimating the yet-to-be calculated higher order QCD correction to a perturbative cross section is to vary both the factorization and renormalization scales by a factor of two up and down compared to the nominal scale. In Fig. 4 we show the variation of the total cross section for t-channel single top production for a range of scales around

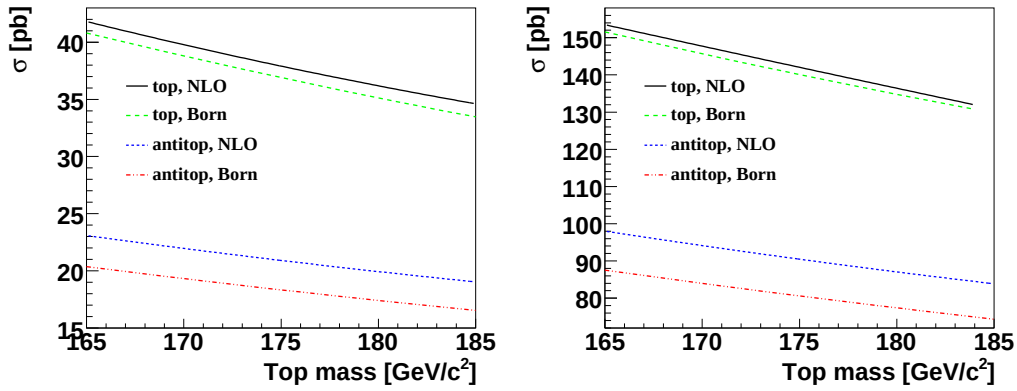

(a) (b)

FIG. 3: Top quark mass dependence of the inclusive t-channel single top quark cross section (a) at 7 TeV and (b) at 14 TeV for the LHC proton-proton collider.

the nominal value $\mu_F = \mu_R = m_t$. [1] The figure shows that the NLO calculation reduces the scale dependence, which can also be seen in Table II.

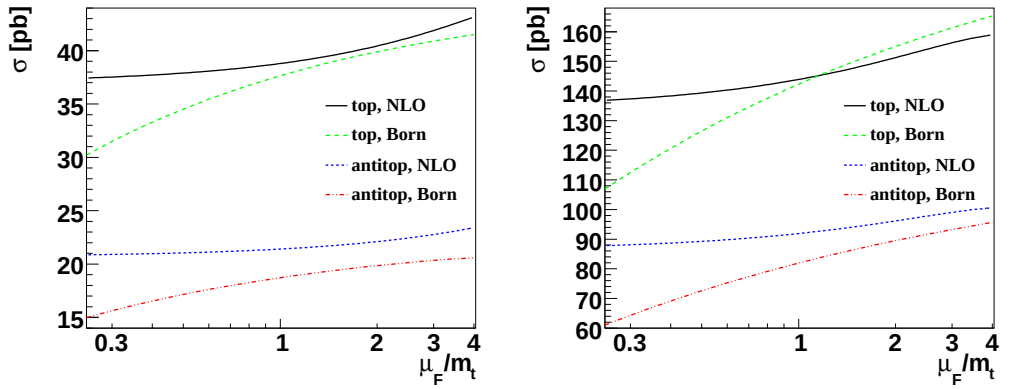

(a) (b)

FIG. 4: Inclusive t-channel single top quark production cross section at a CM energy of (a) 7 TeV and (b) 14 TeV at the LHC for $m_t = 173$ GeV, versus the ratio of the factorization scale μ_F to its typical value $\mu_0 = m_t$.

[1] We vary both scales together in this work, though in general, μ_R and can be varied independently. The difference between using a common scale μ_F $\mu_R = \mu_F$ and independent scales (with the condition $1/2 < \mu_F/\mu_R < 2$) has been studied in the calculation of NLO QCD corrections to the Wt associated production [29, 45], with the result that varying scales independently results in a somewhat larger uncertainty. However, the variation of scale dependence is merely an estimate of the unknown contributions from higher order effects and can only be checked by the complete higher order calculation.

	cross section [pb]	Mass (±1.1 GeV) uncertainty (%)	PDF uncertainty (%)	Scale uncertainty (%)
7 TeV, top, Born	38.6	1.1	0.5	7.1
7 TeV, top, NLO	40.0	1.1	0.5	4.4
7 TeV, antitop, Born	19.1	1.2	0.5	7.2
7 TeV, antitop, NLO	21.9	1.1	0.5	3.9
10 TeV, top, Born	79.1	0.93	0.5	8.6
10 TeV, top, NLO	80.7	0.93	0.5	4.4
10 TeV, antitop, Born	42.6	1.0	0.5	8.8
10 TeV, antitop, NLO	48.7	0.93	0.5	3.9
14 TeV, top, Born	146.5	0.87	0.5	10.0
14 TeV, top, NLO	150.7	0.87	0.5	4.1
14 TeV, antitop, Born	84.3	0.91	0.5	10.0
14 TeV, antitop, NLO	96.1	0.87	0.5	3.7

TABLE II: The top quark mass, PDF and scale uncertainties for the t-channel single top quark production cross section at the LHC for top and antitop quark production, at Born-level and NLO, for a top quark mass of 173 GeV and various LHC CM energies.

Figure 4 also shows that the NLO cross section is below Born-level, except for top quark production with a large scale.

We examine the PDF uncertainty following the standard prescription using the 44 CTEQ Eigenvectors [37, 38]. We evaluate this uncertainty for Born-level and NLO, both top and antitop production, and three different LHC CM energies in Table II. The PDF uncertainty is small and does not change much with top quark mass or collider CM energy.

III. KINEMATIC ACCEPTANCE STUDIES

In this section we explore the final state object kinematics of t-channel single top quark events. We focus on the leptonic decay mode of the W-boson from the top quark decay because those are the focus of the LHC experiments as well [46, 47]. Therefore, the signature of t-channel single top quark events which is accessible experimentally consists of one charged

lepton, missing transverse energy, together with two or three jets. Since we are studying the effects of NLO QCD radiative corrections on the production rate and the kinematic distributions of single top quark events at the parton level in this paper, we do not include any detector effects, such as jet energy resolution or b-tagging efficiency (all jets containing a b quark are b-tagged). Only an approximation of kinematic acceptances of a generic detector are considered. In this section, we first present the event topology of the t-channel single top quark process, and then introduce a jet finding algorithm and the various kinematical cuts used in studying event acceptance. Unless otherwise specified, figures and notation refer to the production of top quarks, and we show antitop quark distributions only when different from those for top quarks. We show distributions for a CM energy of 7 TeV unless otherwise noted.

A. Event topology

At Born-level, the collider signature of the t-channel single top quark process includes two jets (one b-tagged jet from the b quark from the top quark decay, and one non-b-tagged jet from the light quark), one charged lepton, and missing transverse energy ($\not\!\!E_T$) in the final state. This signature becomes more complicated beyond Born-level, as Figure 5 indicates. We use the same notation as in Ref. [24]: the light quark jet is also called "spectator jet", and the label "untagged jet" refers to all jets which do not contain a b or $\bar{b}$ quark.

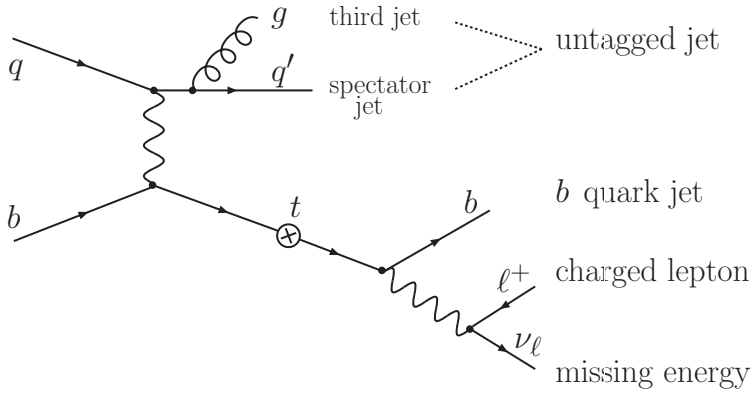

FIG. 5: Pictorial illustration of the t-channel process and the final state notation used in this paper.

At NLO, besides the charged lepton and $\not\!\!E_T$, there may be two jets (one b-tagged jet and

one untagged jet) as for the Born-level, or there may be three jets. The flavor composition of the three-jet final state depends on the origin of the third jet. When it is a gluon or anti-quark (cases (a-c) in Fig. 6), there is one b-tagged jet and two untagged jets. When it is a $\bar{b}$ quark (case (d) in Fig. 6, also called W-gluon fusion), there are two b-tagged jets and one untagged jet. Therefore, prescriptions are needed to identify the b quark jet from the top quark decay and the light quark jet produced with the top quark and to separate them from the additional jet. Additionally, imperfect b-tagging can result in W-gluon fusion events where only one instead of two jets are b-tagged.

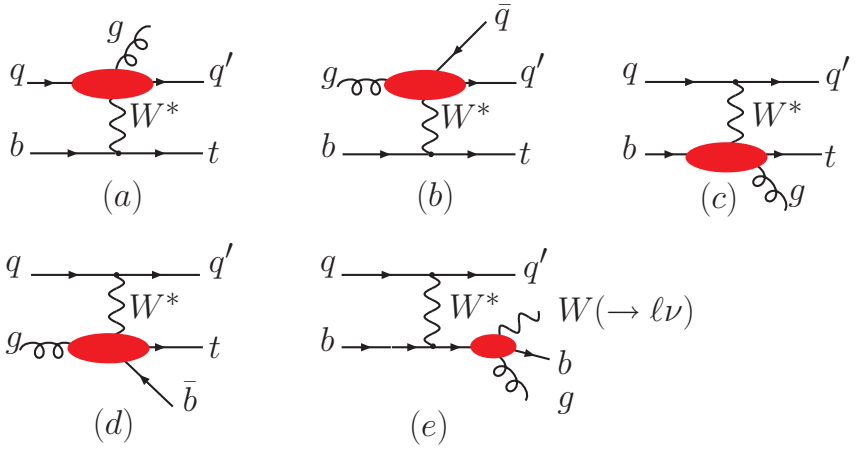

FIG. 6: Representative diagrams of the real emission corrections to t-channel single top quark production: (a) and (b) represent the real radiative corrections to the LIGHT quark line, while (c) and (d) represent the real radiative corrections to the HEAVY quark line, and (e) represents the real radiative corrections to the top quark decay. The NLO QCD corrections are indicated by the large shaded ellipse. Detailed Feynman diagrams can be found in Ref. [22].

The unique signature of the t-channel single top quark process is the spectator jet in the forward direction, and the kinematics of this jet are used to suppress the copious backgrounds from $t\bar{t}$ and $Wb\bar{b}$ production. Studying the kinematics of this spectator jet is important in order to have a better prediction of the acceptance of t-channel single top quark events and of the distribution of several important kinematic variables. In this work, we study the impact of the NLO QCD corrections on the kinematic properties of the spectator jet at the LHC. As pointed out in Ref. [48], in the effective-W approximation, a high-energy t-channel single top quark event is dominated by the fusion diagram of a longitudinal W boson and a b quark. This effective longitudinal W boson is also found in the production of a heavy Higgs

boson via the WW fusion process, hence understanding the effective longitudinal W boson and the kinematics of the light quark jet in t-channel single top quark production is essential to better predict the kinematics of Higgs boson events via WW fusion. We will show that the spectator jet is not uniquely identified anymore at NLO and will compare proposed solutions to this problem. In our Tevatron study [24], we differentiated three categories of events, based on final state jet multiplicity and flavor composition. Here we will explore the same three cases:

1. Born-level-type exclusive two-jet events (containing the b quark and the light quark), which have unique quark-jet assignments because the b-tagged jet is identified as the b quark jet, and the untagged jet is assigned to the spectator jet.

2. Exclusive three-jet events where the additional jet is a gluon. In this case it is straightforward to identify the b quark jet from the top quark decay correctly, but the spectator jet is not uniquely identified anymore.

3. Exclusive three-jet events where the additional jet is a $\bar{b}$ quark. This is the $2 \to 3$ process for which NLO corrections have been calculated [29]. If both of these jets are b-tagged, then the spectator jet is uniquely identified but the b quark jet from the top quark decay is not. If only one of the jets is b-tagged, then both the spectator quark and the b quark from the top quark decay are potentially mis-identified.

We will demonstrate that the fraction of events in these three categories shows significant variation depending on the event reconstruction details.

B. Acceptance

In order to meaningfully discuss the effects of gluon radiation in single top quark events, we must define a jet as an infrared-safe observable. In this study, we adopt the cone-jet algorithm [49] as explained in our previous work [23, 24]. More specifically, we adopt the E-scheme cone-jet approach (4-momenta of particles in a cone are simply added to form a jet) with radius $R = \sqrt{\Delta\eta^2 + \Delta\phi^2}$ in order to define b, q and possibly extra g, $\bar{q}$, or $\bar{b}$ jets, where $\Delta\eta$ and $\Delta\phi$ are the separation of particles in the pseudo-rapidity η and the azimuthal angle ϕ, respectively. In recent studies, the LHC collaborations ATLAS and CMS have used

cone sizes of $R = 0.4$ and $R = 0.5$, respectively [46, 50, 51]. We will consider both in this paper, as well as a larger cone size $R = 1.0$ for comparison. The same R value will also be required for the separation between the lepton and each jet, i.e. lepton isolation.

The kinematic cuts imposed on the final state objects are:

$$\begin{aligned} P_T^\ell \geq 25\,\text{GeV} \;\;,\;\; |\eta_\ell| \leq \eta_\ell^{max}, \\ \not\!\!E_T \geq \not\!\!E_T^{min} \;\;,\;\; E_T^{j1,2} \geq E_T^{j1,2\,min}, \\ E_T^{j3} \geq 15\,\text{GeV} \;\;,\;\; |\eta_j| \leq 5.0, \\ \Delta R_{\ell j} \geq R_{cut} \;\;,\;\; \Delta R_{jj} \geq R_{cut}, \end{aligned} \tag{2}$$

where the jet cuts are applied to both the b- and light quark jets as well as any additional gluon or quark jets in the final state. We consider two different sets of cuts in the following: a loose set of cuts corresponding to the basic experimental event selection, and a tight set of cuts used by the experiments to separate t-channel single top events from the backgrounds. The loose cuts utilize a lepton pseudorapidity corresponding to the full detector,$\eta_\ell^{max} = 2.5$ and require $\not\!\!E_T^{min} = 25$ GeV and $E_T^{j1,2\,min} = 25$ GeV for the leading two jets. The tight cuts restrict leptons to the central detector, $\eta_\ell^{max} = 1.5$, and require $\not\!\!E_T^{min} = 40$ GeV and $E_T^{j1,2\,min} = 50$ GeV for the leading two jets in order to suppress backgrounds. Each event is furthermore required to have at least one lepton and two jets passing all selection criteria. The cut on the separation in R between the lepton and the jets as well as between different jets is given by R_{cut}. In addition, the b quark jet from the top decay is required to be in the central detector ($|\eta^{b\text{–jet}}| < 2.5$), and the other high-$E_T$ jet is required to be at a high pseudo-rapidity, $|\eta^{jet}| > 2.5$.

Table III shows the single top quark production cross sections in pb for the loose and tight set of cuts listed in Eq. (2) for different CM energies and jet cone sizes. The acceptance for the loose cuts is about 4.3%, similar for top and antitop quarks and slightly higher at NLO than at Born-level. Differences between LO and NLO come out when going to the tight set of cuts. From loose to tight, the Born-level top (antitop) quark acceptance goes down by a factor of ten (twelve). The decrease is slightly smaller at NLO and for exclusive 3-jet events. Changing R_{cut} from 0.4 to 0.5 does not change the acceptance very much, but it reduces the number of 3-jet events, mainly because more gluon radiation is clustered into the b quark and light quark jets. For the loose cuts, the increase from Born-level to NLO is comparable to the inclusive cross section increase; whereas for the tight cuts, the

$\sigma \times Br$ [pb]	7 TeV				14 TeV			
	top		antitop		top		antitop	
	LO	NLO	LO	NLO	LO	NLO	LO	NLO
loose cuts, $R_{cut} = 0.4$								
$tq + tqj$	1.66	1.75	0.83	0.96	6.2	6.6	3.6	4.2
tqj		1.28		0.64		5.5		3.2
loose cuts, $R_{cut} = 0.5$								
$tq + tqj$	1.65	1.75	0.82	0.96	6.1	6.6	3.6	4.2
tqj		1.19		0.60		5.1		3.0
tight cuts, $R_{cut} = 0.4$								
$tq + tqj$	0.12	0.14	0.06	0.07	0.61	0.72	0.29	0.36
tqj		0.089		0.05		0.60		0.29
tight cuts, $R_{cut} = 0.5$								
$tq + tqj$	0.12	0.14	0.05	0.06	0.61	0.73	0.29	0.36
tqj		0.084		0.03		0.57		0.27

TABLE III: The t-channel single top (antitop) quark production cross sections times decay branching ratio $t \to bW^+ \to be^+\nu$ ($\bar{t} \to \bar{b}W^- \to \bar{b}e^-\bar{\nu}$) at the 7 TeV and 14 TeV LHC under various cut scenarios listed in the text.

increase from Born-level to NLO is larger, 20% for top quarks and 25% for antitop quarks. This is due to the HEAVY correction, which contributes 20% of the NLO cross section after tight cuts, and is positive for both top and antitop. For the loose set of cuts, the HEAVY correction contributes about 10% of the NLO cross section, again with a positive sign for both top and antitop quarks.

Figure 7(a) shows how the cross section changes as a function of the jet E_T cut when applying the loose set of cuts (without lepton requirements but including a requirement of there being at least two jets in the event). The figure also shows the dependence of the fraction of two-jet events and three-jet events on the jet E_T cut. There are only two-jet events at Born-level, whereas $O(\alpha_s)$ corrections can produce an additional soft jet. The fraction of events with these additional jets is as high as 83% for a jet threshold of 15 GeV (and a jet clustering cone size of 0.4), and drops off to about 10% for a jet threshold of

100 GeV. Since the typical jet E_T thresholds considered by experiments are in the range of 15 GeV to 25 GeV, the fraction of 3-jet events will be very high, and it will be important to study 3-jet t-channel single top quark events at the LHC in detail.

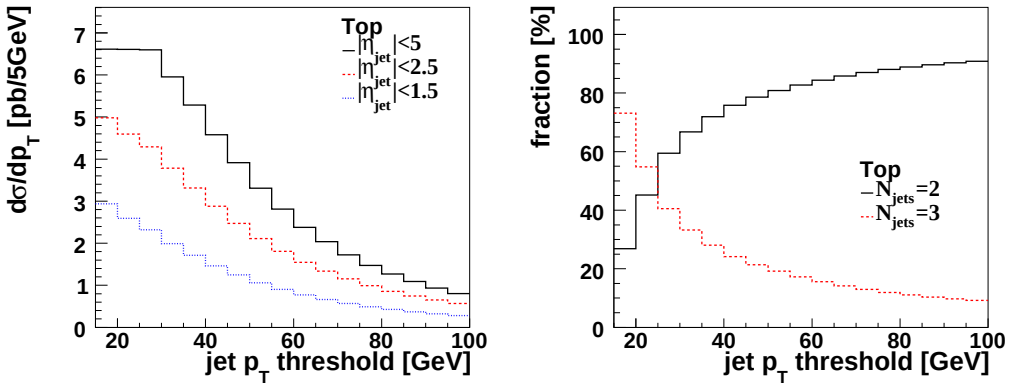

(a) (b)

FIG. 7: Cross section and fraction of three-jet events at the 7 TeV LHC at NLO for varying jet p_T cuts, requiring only that $n_{jets} \geq 2$, and not making any cuts on the electron or neutrino. Shown is the total cross section for events with two or three jets as a function of the jet E_T cut for three different jet pseudo-rapidity cuts (a) and the fraction of two-jet and three-jet events as a function of jet p_T (b). The jet cone size is 0.4 and the lowest threshold considered is 15 GeV.

For antitop quark events the distribution is similar, but the fraction of 2-jet events for the lowest threshold of 15 GeV is higher, 33% (compared to 26% for top quarks). At a CM energy of 14 TeV (10 TeV), the fraction of 2-jet events in top quark production decreases to 17% (21%) as a result of the additional available phase space for gluon radiation.

We will use the loose set of cut values for the following discussion: $\eta_l^{max} = 2.5$, $\eta_j^{max} = 5.0$, and $R_{cut} = 0.4$, $E_{Tj}^{min} = 15$ GeV, cf. Eq. (2).

IV. EVENT DISTRIBUTIONS

In this section we examine the kinematic properties of t-channel single top quark events. The t-channel final state includes one b-tagged jet, one untagged jet, one charged lepton, and missing energy at Born-level, thus it is straightforward to reconstruct the top quark from the b-tagged jet and the reconstructed W boson, and to identify the light quark jet as the untagged jet. At NLO, however, an additional jet can be radiated, which will complicate

the reconstruction of the top quark final state. First, the additional jet can be either a b-tagged jet or an untagged jet. When it is a b-tagged jet, we need to select which of the two b-tagged jets corresponds to the b quark jet from the top quark decay. Here we always choose the highest p_T b-tagged jet. Similarly, when the additional jet is an untagged jet, we need to select which of the two untagged jets is the spectator jet. We will explore two different methods to resolve this ambiguity: selecting the leading untagged jet and selecting the most forward untagged jet. Second, the additional untagged jet can come from either the production or the decay of the top quark. Production-stage emission occurs before the top quark goes on shell, thus the W boson and b quark momenta will combine to give the top quark momentum. Decay-stage emission occurs only after the top quark goes on shell, thus the gluon momentum must also be included in order to reconstruct the top quark momentum properly.

We also examine various kinematic distributions of the final state particles and then study the effects of NLO corrections on distributions concerning the reconstructed top quark, in particular spin correlations between the final state particles. Finally, we explore the impact of the radiated jet in exclusive three-jets events. We use only the loose set of cuts to maximize the efficiency when examining the distributions and efficiencies in detail.

A. Final state object distributions

1. Charged lepton and missing transverse energy

In this section we examine various kinematic distributions of final state objects after event reconstruction and after applying the loose set of cuts, cf. Table I and Eq. (2). We concentrate on inclusive two-jet events in this section because they give more reliable infrared-safe predictions.

Figure 8 show the transverse momentum of the electron and its pseudorapidity as well as the missing transverse energy for top quark events. The antitop quark distributions are very similar. The lepton transverse momentum is typically smaller than the missing transverse energy because the neutrino from the W-boson decay moves preferentially along the direction of the top quark, both for top and antitop quark production. This is due to the left-handed nature of the charged current interaction and can easily be seen when

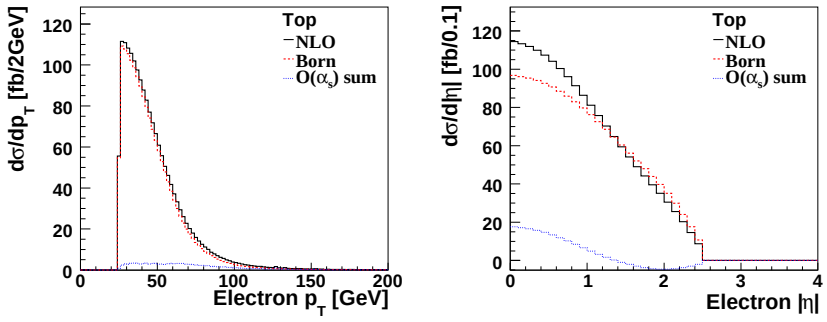

(a) (b)

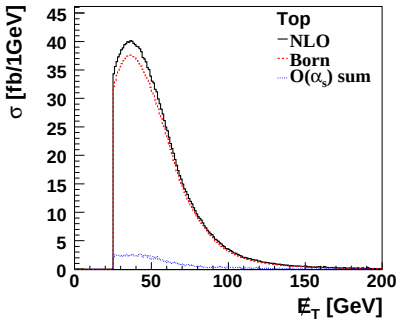

(c)

FIG. 8: (a) transverse momentum of the electron and (b) its pseudo-rapidity and (c) missing transverse energy, after selection cuts, comparing Born-level to $O(\alpha_s)$ corrections, for top quark production at the 7 TeV LHC.

examining the spin correlations between the charged lepton and the top quark in the top quark rest frame. The $O(\alpha_s)$ corrections do not change the distributions much. The pseudo-rapidity distribution of the electron is given in Fig. 8(b). Since the LHC is a proton-proton collider, all pseudorapidity (η) distributions will be symmetric about zero and we thus present distributions of the absolute value $|\eta|$. This distribution is more central for NLO events than for Born-level events because the LIGHT and HEAVY $O(\alpha_s)$ corrections tend to reduce the z-momentum imbalance of the two initial state partons. We will comment more on the subject of angular correlations in Sec. IV D.

2. Spectator jet

One of the unique features of t-channel single top quark production is the light quark jet. This spectator jet can be used to disentangle t-channel single top quark events from

the copious backgrounds. Therefore, its kinematic distributions need to be well studied, especially the impact of $O(\alpha_s)$ corrections. The transverse momentum and energy of the spectator jet are shown in Figure 9.

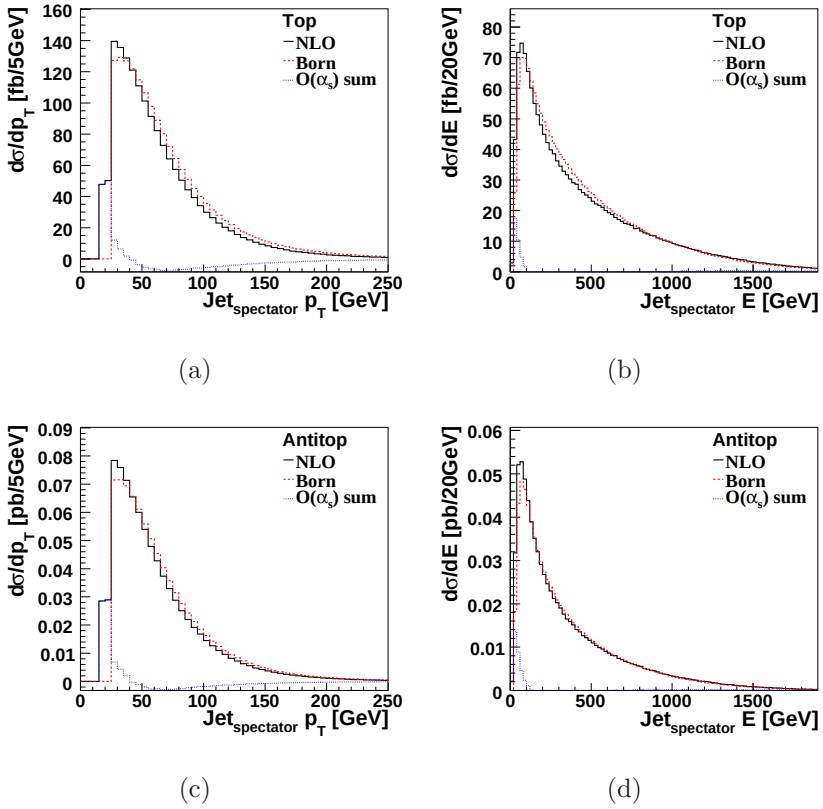

FIG. 9: (a, c) transverse momentum and (b, d) energy of the spectator jet after selection cuts, comparing Born-level to $O(\alpha_s)$ corrections, (a, b) for top quarks and (c, d) antitop quarks at the 7 TeV LHC.

Since the spectator jet comes from the initial state quark after emitting the effective W boson, its transverse momentum peaks around $\sim M_W/2$ as can be seen in Figure 9. The spectator jet p_T distribution in top quark events is slightly higher than in antitop quark events due to the typically harder PDF for up quarks versus down quarks. The $O(\alpha_s)$ corrections lower the transverse momentum and energy distributions of the spectator jet in both cases due to the LIGHT correction. The spectator jet p_T distributions also have a jump at 25 GeV due to events with a spectator jet $p_T < 25$ GeV which fail the loose selection cuts unless a third jet from real emission has $p_T > 25$ GeV. The spectator jet distributions for a CM energy of 14 TeV are similar, except that the tail at high spectator jet energies extends farther.

The pseudo-rapidity distribution of the spectator jet is shown in Figure 10. The distribution is peaked in the forward direction and only few light quark jets appear in the central detector. This is comparable to the Tevatron case which has an asymmetric light quark jet pseudo-rapidity distribution [24, 48]. The $O(\alpha_s)$ corrections shift the spectator jet to even more forward pseudo-rapidities due to additional gluon radiation, though the different contributions have opposite effects. The INIT correction is responsible for the shift to forward pseudo-rapidities due to the additional gluon radiation from the initial state up or down quark. The effect of the HEAVY correction is indirect, though noticeable. The HEAVY correction is largest for central light quark jets because in that case the initial state heavy quark has a higher momentum fraction x. The decay correction has no significant effect on the spectator jet, as expected. Since the $O(\alpha_s)$ corrections are small compared to the Born-level contribution, the overall shift is small. Comparing top to antitop quark production, Figure 10(a) also shows that the antitop quark production cross section is nearly as large as the top quark production cross section in the central region, while the top quark production cross section is significantly larger than the antitop quark one for forward pseudo-rapidities. Central light quark jets come from events where the p_z of the two initial state partons is approximately balanced. This corresponds to small light quark momentum fraction x values, where the difference between up and down quark PDFs is small.

Figure 10(d) compares the spectator jet pseudorapidity distribution for different collider CM energies. As the collider energy goes down, the spectator jet becomes more central and the peak in the forward region is less pronounced because the initial state light quark energy is reduced.

3. b quark jet

Compared to the lepton and $\not\!\!E_T$, the effects of the $O(\alpha_s)$ corrections on the reconstructed b quark jet are more pronounced. Figure 11 shows a comparison of the p_T of the b quark before cuts and the b quark jet after cuts between Born-level and $O(\alpha_s)$ corrections for top quark production. The antitop quark distributions are similar. The p_T distribution of the b quark is predominantly determined by the top quark mass and therefore peaks at $\sim m_t/3$. The NLO QCD corrections shift the peak position to lower values, both at parton level and after selection cuts. At parton level, the only $O(\alpha_s)$ correction that changes the shape is the

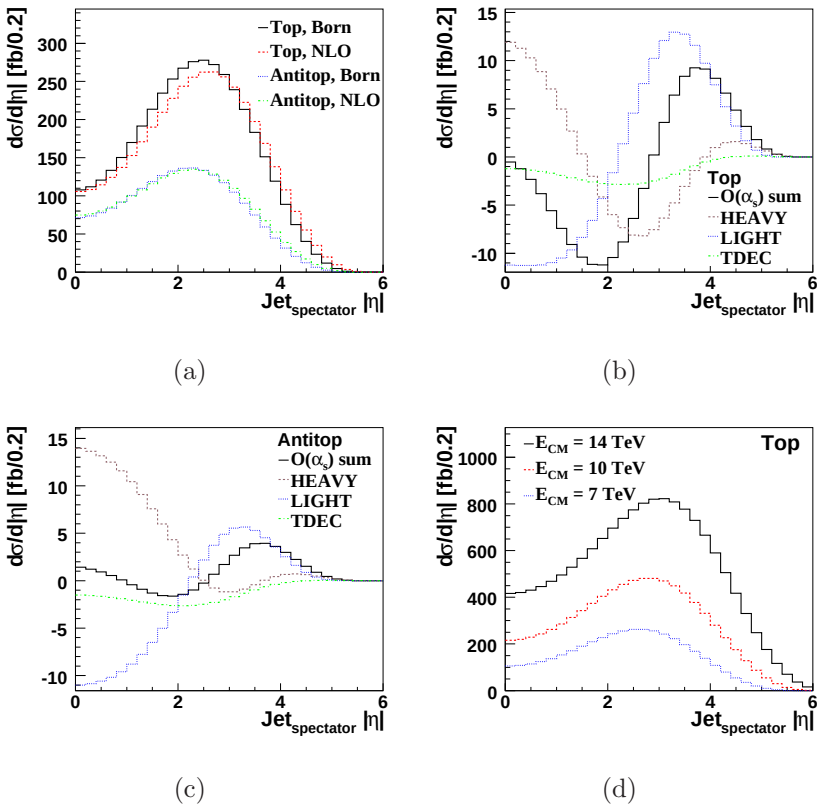

FIG. 10: Absolute value of the spectator jet pseudo-rapidity at the 7 TeV LHC, (a) comparing Born-level to NLO, (b, c) for individual contribution of the $O(\alpha_s)$ corrections for top and antitop quarks, respectively, and (d) for different CM energies for top quarks.

TDEQ correction, which tends to shift the distribution to lower p_T values because a gluon radiated from the top quark decay tends to move along the b quark direction due to collinear enhancements. The LIGHT and HEAVY corrections leave the distribution approximately unchanged and their magnitudes cancel each other.

The selection cuts change the shape of the p_T distribution by removing events in the peak region around 60-70 GeV. For these events the top quark is produced with low p_T, hence the light quark also has low p_T and the events fail the requirement of at least two jets. The selection cuts also affect the $O(\alpha_s)$ corrections shown in Fig. 11(d). The TDEC correction is the largest contribution, similar to the parton level in Fig. 11(b), and it also shows the effect of the selection cuts because the top quark and thus light quark p_T is unchanged. The HEAVY correction shows a similar behavior; because it is an initial state correction it does not change the p_T balance between light quark and top quark. Real gluon emission in the LIGHT correction does change this balance, thus the effect is not visible as clearly anymore.

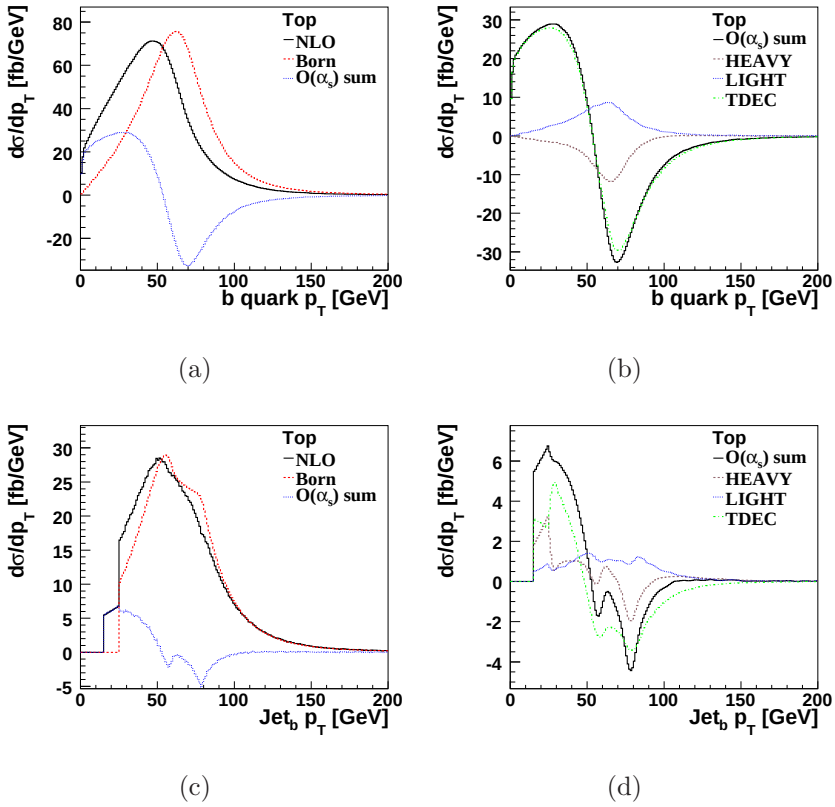

FIG. 11: Transverse momentum of (a, b) the b quark before selection cuts and (c, d) the b quark jet after cuts, (a, c) comparing Born-level to $O(\alpha_s)$ corrections and (b, d) the individual $O(\alpha_s)$ contributions, at the 7 TeV LHC.

The b quark jet pseudo-rapidity distribution in top quark events is less affected by the $O(\alpha_s)$ corrections, as can be seen in Fig. 12. The top quark is so heavy that it is mostly produced in the central rapidity region and thus the b quark jet from its decay also peaks around a pseudo-rapidity of zero. The shape of the b quark jet pseudo-rapidity distribution remains almost unchanged compared to the Born-level because it comes from the top quark decay. The difference between Born-level and $O(\alpha_s)$ is larger for antitop quark events. While the Born-level contribution and the LIGHT corrections are smaller for antitop quarks, the HEAVY and TDEC corrections are similar in size for top and antitop quarks. These distributions are similar at a CM energy of 14 TeV.

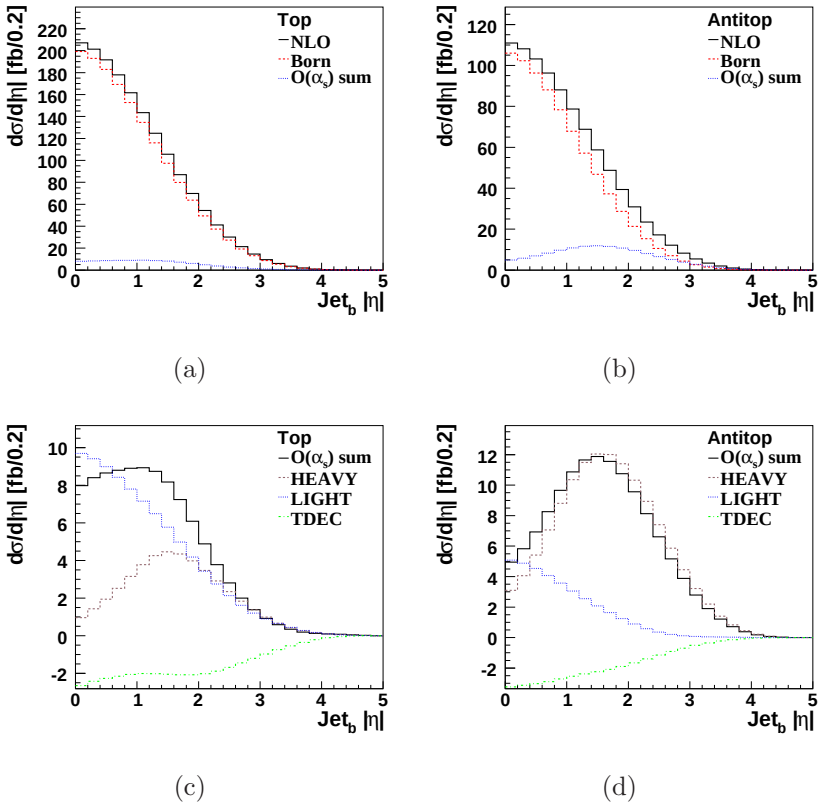

FIG. 12: Pseudo-rapidity of the b quark jet after selection cuts at the 7 TeV LHC, (a, b) comparing Born-level to $O(\alpha_s)$ corrections and (c, d) individual $O(\alpha_s)$ contributions, in (a, c) for top quarks and in (b, d) for antitop quarks.

4. Event kinematics

The impact that different $O(\alpha_s)$ corrections have on the p_T of the jets is also reflected in event-wide energy variables such as the total transverse energy in the event (H_T) or the reconstructed invariant mass of all final state objects. The total transverse energy is defined as

$$H_T = p_T^{lepton} + \not{E}_T + \sum_{jets} p_T^{jet}. \tag{3}$$

The distribution of H_T for t-channel single top quark events is shown in Fig. 13. The Born-level H_T distribution peaks around 200 GeV at a CM energy of 7 TeV and shifts to slightly higher values for larger CM energies. The HEAVY contribution decrease the height of the peak and shifts it to higher values, while the LIGHT and TDEC contributions are small. All three $O(\alpha_s)$ contributions broaden the distribution. The antitop quark production distributions as well as those for lower CM energies are very similar because the shape is

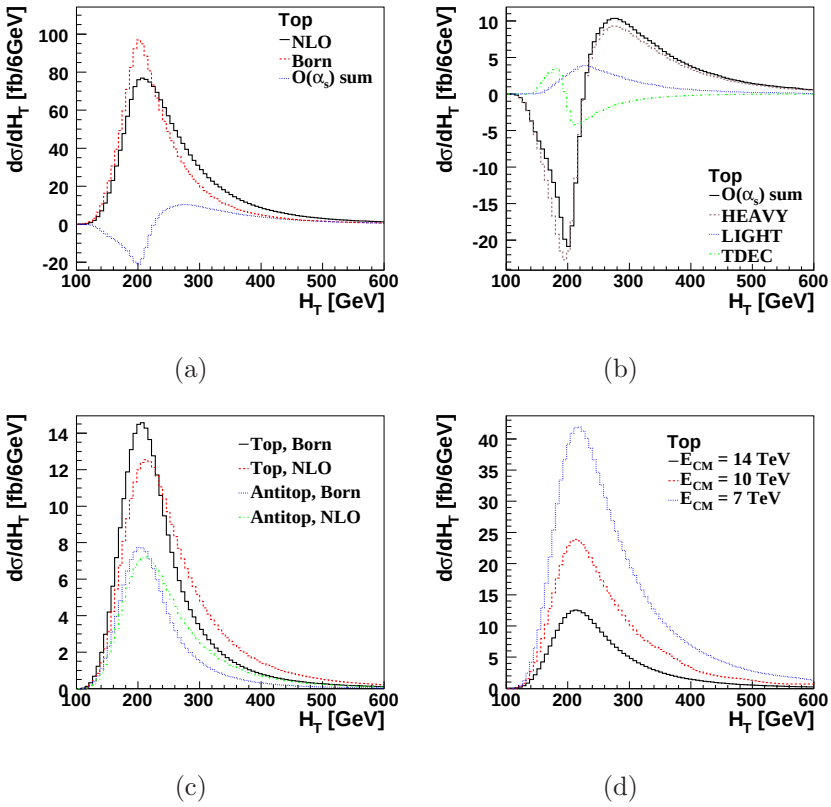

FIG. 13: Total event transverse energy H_T after selection cuts, (a) comparing Born-level to $O(\alpha_s)$ corrections and (b) the individual $O(\alpha_s)$ contributions, (c) comparing top to antitop quark production, for top quark production at the 7 TeV LHC, and (d) comparing different CM energies.

determined mainly by the top quark mass.

B. Distributions for three-jet events

As Fig. 7 shows, the majority of t-channel events at the LHC contain three reconstructed jets rather than two. This is the main difference between t-channel single top quark production at the Tevatron and the LHC, other than that the LHC collider is not CP symmetric. This is also true for events passing the loose selection cuts. In this section we focus on the properties of these three-jet events and specifically the additional jet. As expected, the effect is not quite as large when only jets within a very small η range are considered because the extra jet typically has higher η. In order to study $O(\alpha_s)$ effects it is thus important to set the jet η cut as high as possible and the jet E_T cut as low as possible.

1. Abundance of three-jet events

Additional light quark jets arise in the LIGHT quark line corrections, in the TDEC corrections, and in the gluon radiation diagrams of the HEAVY correction. An additional b-tagged jet arises as the $\bar{b}$ quark in the W-gluon fusion HEAVY process. Since we assume fully efficient, perfect b-tagging we consider events with one b-tagged jet and two b-tagged jets separately. This separation is reduced if the b-tagging efficiencies is less than 100% and some of the W-gluon fusion HEAVY events only have one b-tagged jet.

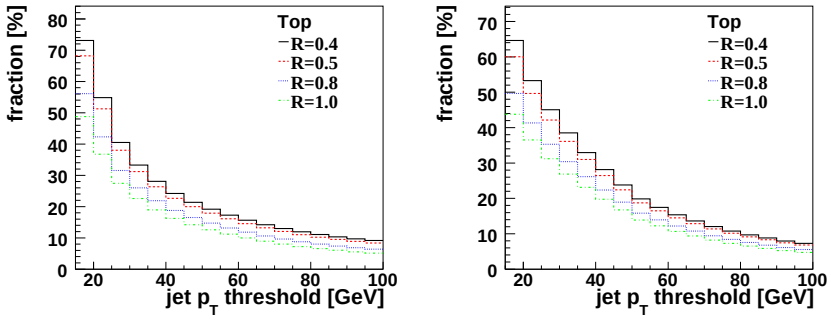

(a) (b)

FIG. 14: Fraction of 3-jet events as a function of the jet p_T threshold at the 7 TeV LHC for different jet cone sizes, (a) for the loose set of cuts and (b) for the tight set of cuts.

From Fig. 7 it is clear that the jet multiplicity at NLO depends strongly on the jet p_T cut. Figure 14 shows that it also depends on the jet reconstruction cone size. The dependence of the total cross section on the jet pseudo-rapidity cut is different between Born-level and NLO, mostly as a result of the presence of a third jet.

Figure 15 compares the momentum of the b quark jet from the top quark decay and the $\bar{b}$ quark from the HEAVY correction and examines the fraction of events containing one or two b-tagged jets in the final state. Events with both b and $\bar{b}$ jets originate from the W-gluon fusion sub-process, $qg \to q'\bar{b}t(\to bW(\to \ell^+\nu))$. The fraction of events with two b-tagged jets is about 40% for low jet p_T, and remains high even for higher jet p_T. Even for jet p_T above 100 GeV, the fraction of events with both a b and a $\bar{b}$ jet is above 10%. Figure 15 also shows that for exclusive three-jet events, the fraction of events with two b-tagged jets is even higher. The fraction of b-tagged jets also depends on the jet $|\eta|$ threshold, as shown in Fig. 15(c). Since the $\bar{b}$ quark from the W-gluon fusion sub-process typically moves in the forward direction, a high $|\eta|$ threshold results in two b-tagged jets per event, whereas a low

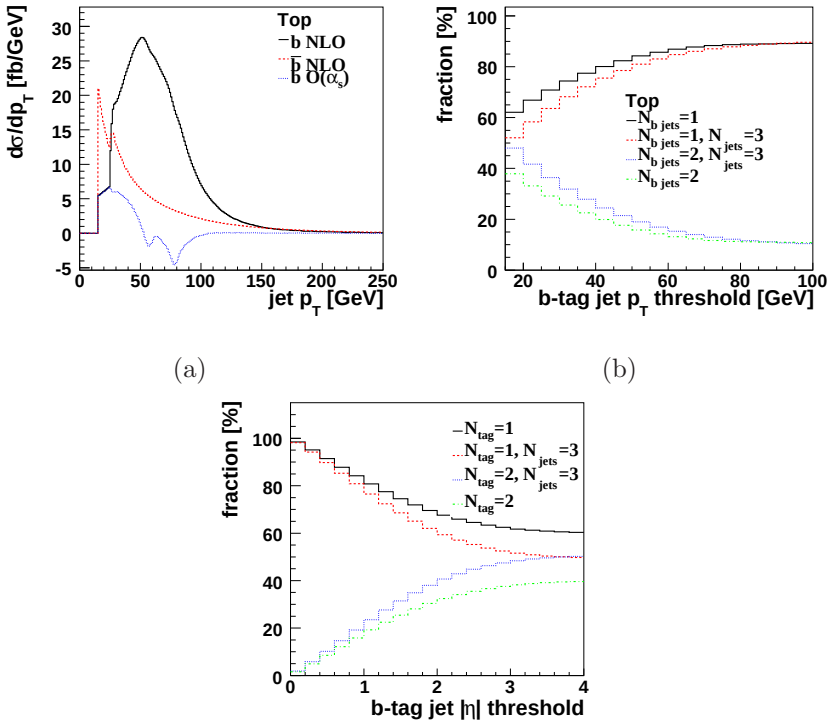

FIG. 15: (a) p_T of the b and $\bar{b}$ jets in top quark production, (b) fraction of events with one or two b-tagged jets as a function of jet p_T threshold and (c) as a function of jet $|\eta|$ threshold, for both inclusive two-jet and exclusive three-jet events, at the 7 TeV LHC.

jet $|\eta|$ threshold results in only one.

2. *Third jet*

Here we consider the kinematic distribution of the third jet and its flavor composition.

Figure 16 shows the transverse momentum and pseudo-rapidity of the different contributions to the third jet. The HEAVY correction is broken up into its two components, one where the third jet originates from a gluon (Fig. 6 (c)) and one where the third jet originates from a $\bar{b}$-quark (W-gluon fusion, Fig. 6 (d)). The $\bar{b}$-quark case accounts for about half of the total 3-jet cross section, more at higher p_T and higher $|\eta|$. The gluon case accounts for about 15% of the total 3-jet cross section, but the gluon jet is more central and typically at lower p_T. The LIGHT correction shows the same forward pseudo-rapidity peak as the spectator jet (as expected) and contributes about 23%. The TDEC correction contributes about 12%,

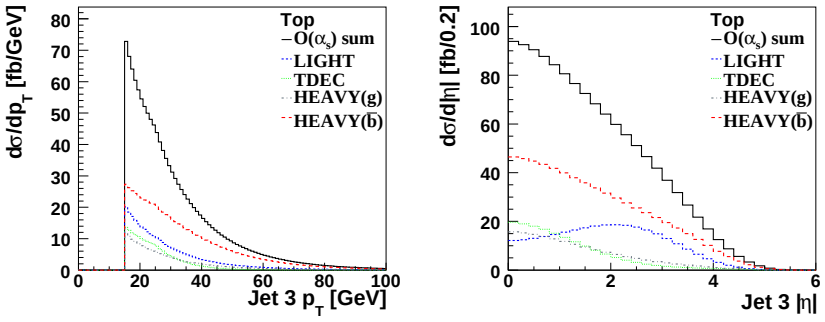

(a) (b)

FIG. 16: Third jet (a) p_T and (b) $|\eta|$ for loose selection cuts in top quark production at the 7 TeV LHC.

mostly at low p_T and in the central pseudo-rapidity region. This limited range is the direct result of the phase space available to the b-quark in the top quark decay. Fig. 16 shows that all of the contributions are important and none can be neglected when modeling t-channel events. While the conventional wisdom that W-gluon fusion dominates the t-channel holds true, nevertheless all diagrams contribute.

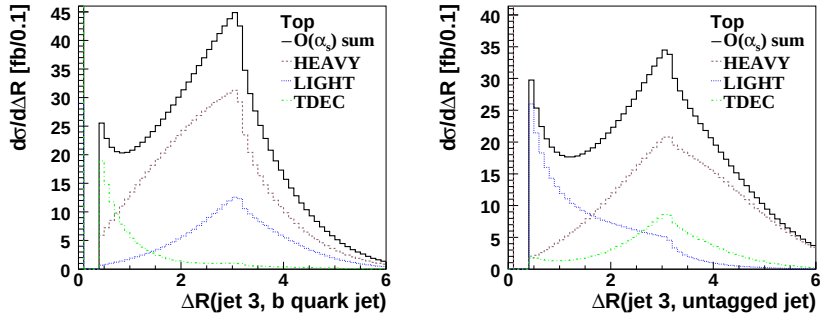

(a) (b)

FIG. 17: Separation between the third jet and (a) the tagged jet and (b) the untagged jet after selection cuts for the various $O(\alpha_s)$ corrections at the 7 TeV LHC.

Normally an extra jet from decay-stage radiation should be included in the top quark reconstruction in order to include all top quark decay products. Figure 17(a) shows that jets from the TDEC contribution are close to the b quark jet, thus at least in principle easily identified. Extra jets from the production-stage radiation (LIGHT and HEAVY corrections) are typically farther away from the b-tagged jet. However, the HEAVY correction is large, significantly larger than the TDEC correction for ΔR values larger than about 0.8. The

higher p_T cuts for the tight selection make this situation worse because they increase the relative size of the production emission, and the situation is similar for antitop quarks and for higher CM energies. Decay-stage radiation can more easily be identified when an additional top mass constraint is used to choose a jet pairing, see section IV C.

Figure 17(b) shows the equivalent distribution in ΔR between the extra jet and the untagged jet. In this case the LIGHT radiation peaks close to the untagged jet as expected from gluon radiation in the final state. There is an additional LIGHT contribution at higher ΔR from production-stage radiation of the light quark line.

Note that there are entries at zero in the distributions in Fig. 17. These corresponds to events where the third jet is the leading b-tagged jet (i.e. there are two higher p_T untagged jets) or the leading untagged jet (i.e. there are two higher p_T tagged jets). The third jet corresponds to the b-tagged jet in 13% (12%) of the top (antitop) quark events. It corresponds to the untagged jet in 17% (18%) of the top (antitop) quark events.

3. Identifying the spectator jet in 3-jet events

In events containing two untagged jets, it is not clear which of the two is the light quark jet and which is the gluon (or $\bar{b}$-quark) jet. Two approaches are currently in use: choosing the more forward jet in pseudo-rapidity (as used for example by the LHC experiments ATLAS and CMS, see section 3.4 in Ref. [46]), and choosing the highest-p_T jet that is not b-tagged (as used for example by the Tevatron collaborations DØ [8, 11] and CDF [12]). Here we explore the accuracy of these two methods, i.e. the fraction of events for which the light quark jet is correctly identified in 3-jet events by each algorithm.

Figure 18 shows the p_T of the untagged jet for these two cases, together with its composition in terms of spectator jet or gluon jet. When the highest $|\eta|$ jet is chosen, the spectator jet is correctly identified in only 80% of the events. By contrast, when the highest p_T jet is chosen, it is correctly identified in 92% of the events after loose cuts. These efficiencies are similar for antitop files and about 2% lower at a CM energy of 14 TeV. Figure 18 shows that for untagged jet p_T above 70 GeV, the correct jet is chosen in 95% of the events, approaching 100% as the jet p_T increases.

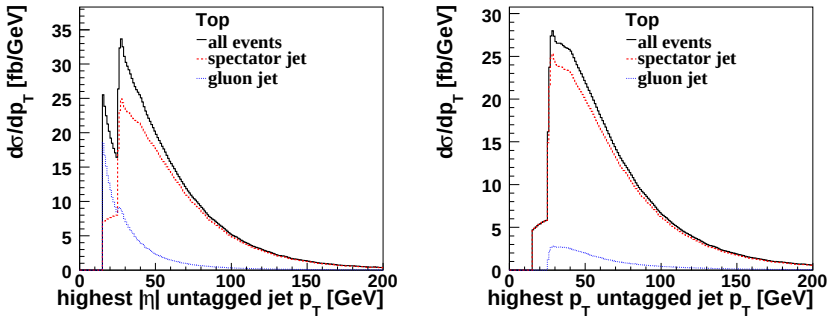

(a) (b)

FIG. 18: Transverse momentum of the untagged jet that is (a) highest in $|\eta|$ and (b) highest in p_T, for all events and separately for those where it is the spectator jet or a gluon jet, at the 7 TeV LHC.

4. Identifying the b quark jet in 3-jet events

At Born-level, there is only one b-tagged jet, which is identified with the b quark from the top quark decay. In events containing both a b quark and a $\bar{b}$ quark, this unambiguous association is not possible anymore. However, the additional jet typically has lower p_T than the b-quark from the top quark decay, we therefore choose the highest p_T b-tagged jet as the b quark from the top quark decay.

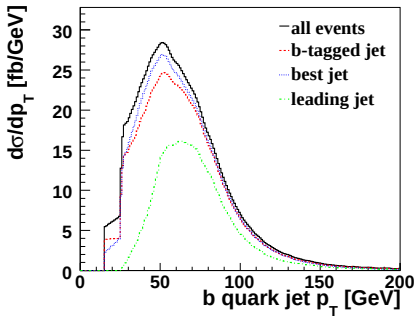

(a)

FIG. 19: Transverse momentum of the b quark jet, for all events and for different b quark jet reconstruction choices, after selection cuts at the 7 TeV LHC.

Figure 19 shows the p_T of the b quark jet from the top quark decay, for all events and for three different algorithms to identify the b quark jet: a) choosing the leading jet in the event (highest p_T), b) choosing the leading b-tagged jet, and c) choosing the jet or jet pair that,

when combined with the reconstructed W boson, gives a top quark mass closest to 173 GeV. The overall fraction of correctly identified b quark jets is 49% for the leading jet, 87% for the leading b-tagged jet and 90% for the best jet, for top quark production. These fractions for antitop quarks are 40%, 83% and 91%, respectively, slightly lower for the leading jet and the leading b-tagged jet and unchanged for the best jet. They are similar for higher CM energies and different cone sizes. Algorithm a) is the most inefficient because there are two high-p_T jets in each event. Simply choosing the leading b-tagged jet is an obvious choice but requires b-tagging which reduces the acceptance. Algorithm c) improves upon b) slightly because it also accounts for decay-stage radiation by considering a two-jet system as the b quark jet. We can investigate this decay-stage radiation further by looking only at events where a two-jet system is chosen. Figure 20 shows the angle between the two jets in this case, where both have been boosted into the top quark rest frame.

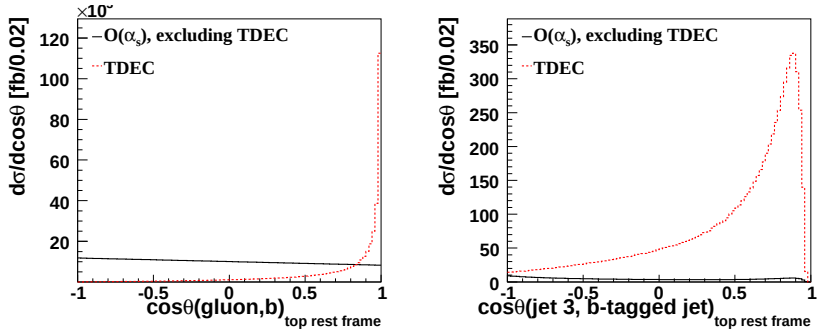

(a) (b)

FIG. 20: Cosine of the angle (a) between the gluon from the TDEC radiation and the b quark from the top quark decay and (b) between the third jet and the b-tagged jet if the third jet is included in the top quark reconstruction, both in the top quark rest frame, after selection cuts at the 7 TeV LHC.

Figure 20 shows that in those events in which the third jet is included in the top quark reconstruction it is close in angle to the b-quark from the top quark decay as expected. At the parton level, shown in Fig. 20(a), decay-stage radiation peaks very closely to the b quark from the top quark decay, and is clearly distinguishable from the other $O(\alpha_s)$ corrections. After event reconstruction and selection, the $cos\theta$ distribution for decay radiation is broader, but still clearly peaks in the direction aligned with the b-tagged jet.

Nevertheless, the difference between algorithm b) and c) is small, and moreover algorithm

c) will do worse when detector resolution effects are included. Choosing the leading b-tagged jet does not suffer from detector resolution problems and is almost as efficient. We will therefore identify the leading b-tagged jet with the b quark jet from the top quark decay for the remainder of this paper.

C. Top quark reconstruction

The complete reconstruction of the single top quark final state, including the W boson and the top quark itself, is necessary in order to not only take advantage of simple single-object kinematics but also of correlations between objects when separating the signal from the backgrounds. We use parton-level information for the W boson, i.e. we reconstruct it from the lepton and the neutrino. Experimentally, the z momentum of the neutrino (p_z^ν) is not known and typically obtained from a W boson mass constraint. Here we use the parton-level p_z^ν to focus our studies on the effects of jet-related processes. We then combine the W boson with the leading b-tagged jet to form the top quark.

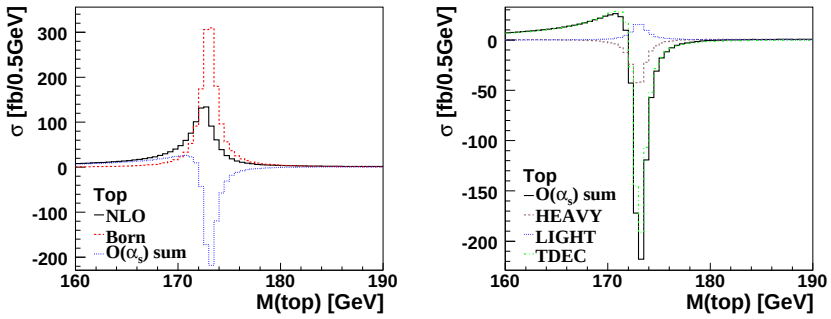

(a) (b)

FIG. 21: Invariant mass of the W boson and the leading b-tagged jet at the 7 TeV LHC, (a) comparing Born-level to NLO and (b) the individual $O(\alpha_s)$ corrections.

Figure 21 shows the invariant mass of the reconstructed top quark for the different $O(\alpha_s)$ corrections. As expected, the LIGHT and HEAVY corrections do not impact the shape of the invariant mass distribution. The TDEC correction shifts the invariant mass to lower values due to real-emission events where the additional jet is not included in the top quark reconstruction.

Figure 22 shows the transverse momentum distribution of the reconstructed top quark. At Born-level, this is identical to the spectator jet p_T, but at $O(\alpha_s)$ additional real emission

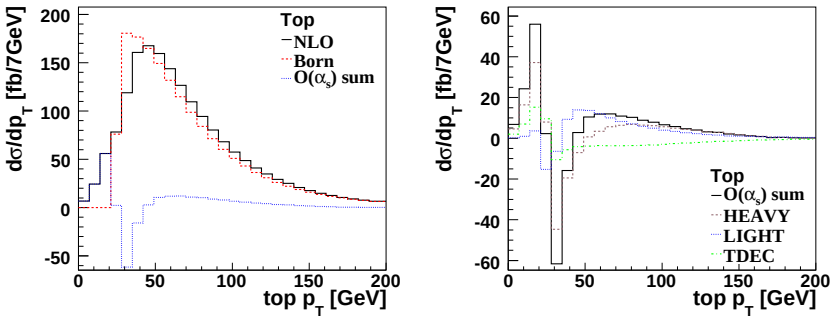

(a) (b)

FIG. 22: Transverse momentum of the reconstructed top quark, (a) comparing Born-level to $O(\alpha_s)$ corrections and (b) the individual $O(\alpha_s)$ contributions at the 7 TeV LHC.

changes that. TDEC emission shifts the top quark p_T down, whereas LIGHT and HEAVY emission tend to shift it up. The distributions for antitop quarks and different CM energies are similar.

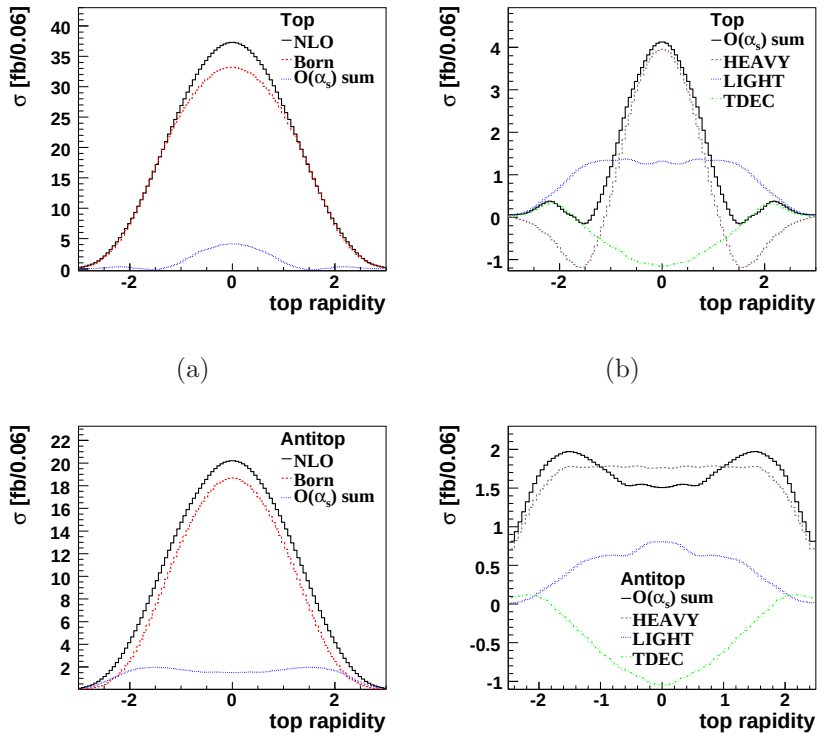

(a) (b)

(c) (d)

FIG. 23: Rapidity of the top quark after selection cuts, (a, c) comparing Born-level to $O(\alpha_s)$ corrections and (b, d) the individual $O(\alpha_s)$ contributions, for (a, b) top quarks and (c, d) antitop quarks produced at the 7 TeV LHC.

Figure 23 compares the rapidity of the top quark after selection cuts between top and antitop quark production. For top quark production, shown in Figs. 23(a) and (b), the HEAVY corrections shift the top quark to more central rapidities, similar to the light quark pseudorapidity distribution in Fig. 10. The LIGHT and TDEC corrections have little to no effect as expected. The rapidity distribution is more narrow in antitop quark production due to the smaller parton momentum fraction of the incoming down quark compared to the incoming up quark that results in a top quark. At NLO, the top quark rapidity distribution is widened, while the antitop quark rapidity distribution is only shifted up in magnitude. This is mainly a result of the different contributions from the HEAVY correction in the two cases. This difference between top and antitop quark production is similar for different CM energies.

D. Top quark polarization

In this section we study angular correlations expected from event kinematics, reconstructing the top quark using the leading b-tagged jet and the W boson. Since single top quark production in the SM is a weak interaction process, the top quark is highly polarized in a suitable basis, and this polarization can be measured. Detailed studies of the top quark polarization and of angular correlations in the top quark electroweak coupling to other particles is a sensitive probe to new physics [1]. The spin correlations were also recently explored at the parton level for the 14 TeV LHC [52]. Here we study angular correlations between top quark production and decay. In particular the charged lepton is maximally correlated with the top quark spin [53, 54]. We can thus obtain the most distinctive distribution by plotting the angle between the charged lepton and the spin axis of the top quark in its rest frame.

Three different axes for the spin polarization have been studied, each in the top quark rest frame: the helicity basis, the spectator basis, and the beamline basis [54]. Figure 24 illustrates the production and decay of the top quark from a spin correlation perspective, with the top quark at rest in the center of the figure. Just as the lepton from the top quark decay is maximally correlated with the top quark spin, so is the down-type quark in the top quark production. This down-type quark typically corresponds to the spectator quark in t-channel top quark production. Hence the spectator basis should produce the largest spin

correlation for top quark production. In the beamline basis, the top quark spin is measured along the direction of one of the incoming protons. In t-channel antitop quark production the down-type quark typically comes from one of the two incident protons, but since the LHC is a proton-proton collider, a choice of direction needs to be made. It has been proposed to simply choose the proton that is most likely to have produced the spectator jet based on the sign of η of the spectator jet [54]. Here we also explore choosing based on the sign of p_z of the c.m. system. In the commonly used helicity basis, the top quark spin is measured along the top quark direction of motion in the center of mass frame, which is chosen as the frame of the (reconstructed top quark, spectator jet) system after event reconstruction. We will examine all three bases for both top and antitop quark production here.

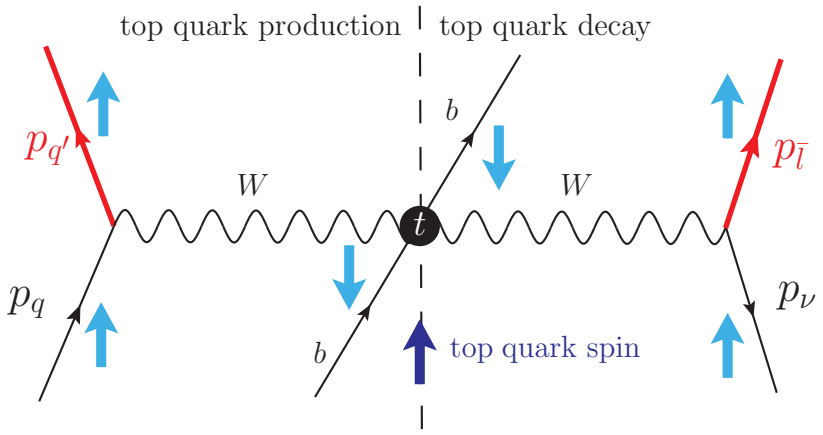

FIG. 24: Illustration of the spin correlation between top quark production and top quark decay. The circle denotes the top quark rest frame and light colored arrows indicate the spin direction.

In the helicity basis, the c.m. frame needs to be reconstructed in order to define the top quark momentum direction. This is straightforward at Born-level but complicated by additional jet radiation at NLO. Therefore, choosing the appropriate frame is necessary to maintain the best spin correlation. In this study, two options for reconstructing the c.m. frame are investigated:

1. $tq(j)$-frame: the c.m. frame of the incoming partons. This is the rest frame of all the final state objects (reconstructed top quark and all others jets). In exclusive three-jet events, this frame is reconstructed by summing over the 4-momenta of top quark, spectator jet and third-jet.

2. tq-frame: the c.m. frame of the top quark and spectator jet. In this case, even in exclusive three-jet events, the reference frame is constructed by summing over only the 4-momenta of the top quark and spectator jet.

In exclusive two-jet events, the two frames are identical, they only differ for exclusive three-jet events. At the Tevatron, it was found that the tq-frame gives a larger degree of polarization. This is also true at the LHC as shown in Table IV and discussed below. We therefore choose the tq-frame when calculating the top quark polarization in the helicity basis.

In the helicity basis, the polarization of the top quark is examined as the angular distribution ($\cos\theta_{hel}$) of the lepton in the top quark frame relative to the moving direction of the top quark in the c.m. frame. The angular correlation in this frame is given by

$$\cos\theta_{hel} = \frac{\vec{p}_t \cdot \vec{p}_\ell^{\,*}}{|\vec{p}_t||\vec{p}_\ell^{\,*}|}, \tag{4}$$

where $\vec{p}_\ell^{\,*}$ is the charged lepton three-momentum defined in the rest frame of the top quark, whose three momentum is denoted as $\vec{p}_t$, which is in turn defined in the c.m. frame. For a left-handed top quark, the angular correlation of the lepton ℓ^+ is given by $(1-\cos\theta_{hel})/2$, and for a right-handed top quark, it is $(1+\cos\theta_{hel})/2$. Figure 25(a) shows that this linear relationship for $\cos\theta_{hel}$ is indeed a valid description for t-channel single top quark events at the parton level. The figure also shows that the top quark is almost completely polarized in the helicity basis at Born-level, and that this polarization is weakened when including $O(\alpha_s)$ corrections. Figure 25(b) shows that this weakening is amplified after event reconstruction, where the effect of the lepton-jet separation cut can also be seen, as the drop-off of the $\cos\theta_{hel}$ distribution close to a value of -1. This corresponds to the events in which the top quark is back-to-back with the lepton, hence the spectator jet is aligned with the lepton.

In the spectator basis, the relevant angular correlation for the t-channel process is $\cos\theta_{spec}$, defined as

$$\cos\theta_{spec} = \frac{\vec{p}_{spec}^{\,*} \cdot \vec{p}_\ell^{\,*}}{|\vec{p}_{spec}^{\,*}||\vec{p}_\ell^{\,*}|}\,, \tag{5}$$

where $\vec{p}_{spec}^{\,*}$ is the spectator jet three-momentum in the top quark rest frame and $\vec{p}_\ell^{\,*}$ is the lepton three-momentum in the top quark rest frame. For top quark production, this basis picks the wrong spin axis direction for the $\bar{d}b$ and $b\bar{d}$ initial states, but as pointed out in Ref. [54], the spectator jet is almost parallel to the initial state light quark, thus some spin correlation is preserved even in that case. At Born-level the polarization is identical between

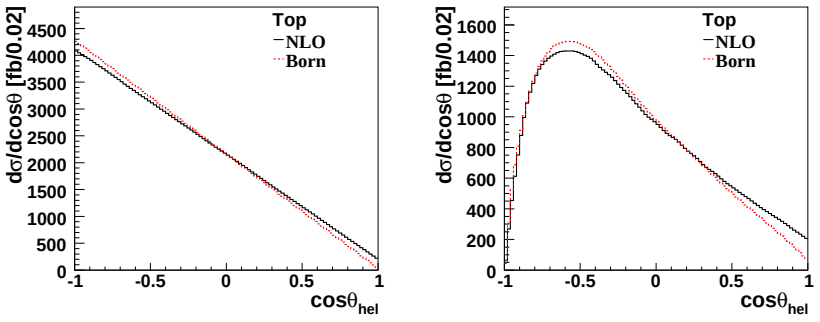

(a) (b)

FIG. 25: Top quark polarization in the helicity basis, (a) using the full parton information and (b) after event reconstruction with selection cuts, comparing Born-level to NLO (normalized to Born-level), at the 7 TeV LHC.

the helicity basis and the spectator basis because the spin quantization axes point in opposite directions (in the c.m. frame, the light quark and the top quark are back-to-back). This is also true at NLO when the tq frame is used as the c.m. frame.

In the beamline basis, the relevant angular correlation for the t-channel process is $\cos\theta_{beam}$, defined as

$$\cos\theta_{beam} = \frac{\vec{p}_p^{\,*} \cdot \vec{p}_\ell^{\,*}}{|\vec{p}_p^{\,*}||\vec{p}_\ell^{\,*}|}\,, \tag{6}$$

where $\vec{p}_p^{\,*}$ is the three-momentum of one of the protons in the top quark rest frame and $\vec{p}_\ell^{\,*}$ is the lepton three-momentum in the top quark rest frame. For a top quark polarized in the positive z-direction, the angular distribution of the lepton ℓ^+ is $(1+\cos\theta_{beam})/2$, while for a top quark polarized in the negative z-direction it is $(1-\cos\theta_{beam})/2$. Since the LHC is a proton-proton collider, it is unknown which of the two protons provided the light quark in each event. Three different approaches are explored here to solve this ambiguity: a) choosing the positive z-direction for every event (simply called beamline basis), b) choosing the z-direction of the spectator quark (η beamline basis) [54], and c) choosing the z-direction of the c.m. frame of all particles in the lab frame ($\hat{s}$ beamline basis). Figure 26 shows the linear relationship for $\cos\theta_{beam}$ in the beamline basis. The distribution is much more flat than that in the helicity basis, and Fig. 26 demonstrates that the $\hat{s}$ beamline basis and the η beamline basis both significantly improve this situation because the correct down-quark direction is picked more often. After event reconstruction the situation is similar: the spin correlation is further reduced and shows a drop-off close to one due to the limited lepton

η range.

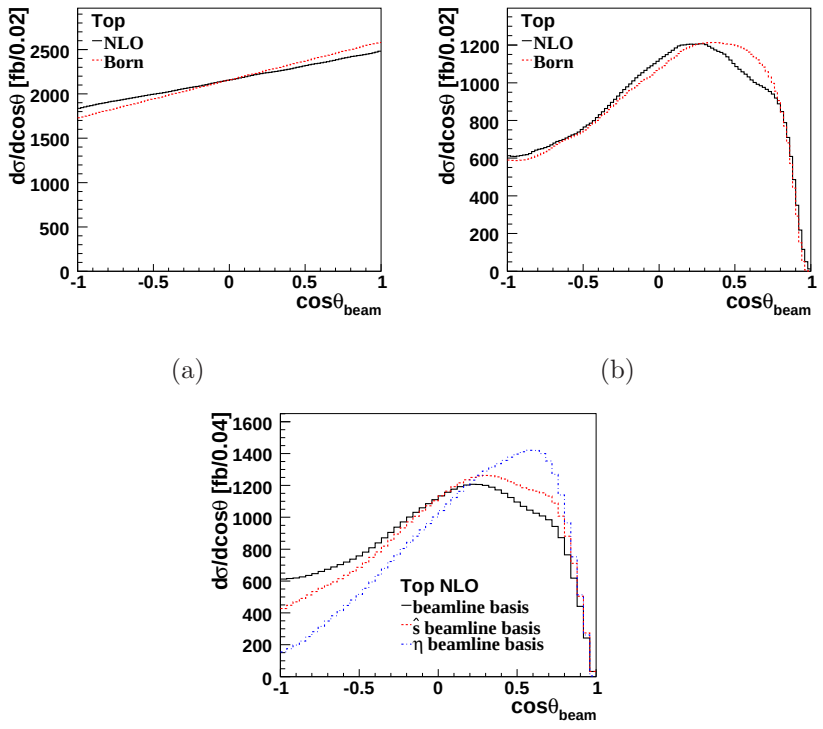

FIG. 26: Top quark polarization (a, b) in the beamline basis, (a) using parton information and (b) after event reconstruction with selection cuts, comparing Born-level to NLO (normalized to Born-level). (c) comparison of the beamline basis to the $\hat{s}$ beamline basis and the η beamline basis at the 7 TeV LHC.

To better quantify the change in polarization, it is useful to define the degree of polarization $\mathcal{D}$ of the top quark. This is given as the ratio

$$\mathcal{D} = \frac{N_- - N_+}{N_- + N_+},$$

where N_- (N_+) is the number of left-handed (right-handed) polarized top quarks in the helicity basis. Similarly, in the spectator (beamline) basis, N_- (N_+) is the number of top quarks with polarization against (along) the direction of the spectator jet (proton) three momentum in the top quark rest frame. The angular distribution is then given by [55]

$$\begin{aligned} \frac{1}{\sigma}\frac{d\sigma}{d(\cos\theta)} &= \frac{N_-}{N_- + N_+}\frac{1+\cos\theta}{2} + \frac{N_+}{N_- + N_+}\frac{1-\cos\theta}{2} \\ &= \frac{1}{2}\left(1 + D\cos\theta_i\right). \end{aligned}$$

Simple algebra leads to the following identity:

$$\mathcal{D} \;=\; -3\int_{-1}^{1} x\,\frac{d\sigma}{\sigma dx}\,dx\,, \tag{7}$$

where $\dfrac{d\sigma}{\sigma dx}$ is the normalized differential cross section as a function of the polar angle x. Here, x denotes $\cos\theta_{hel}$ in the helicity basis, etc. The polarization fraction and asymmetry are not given here but can be calculated easily from the numbers provided [24].

Table IV shows $\mathcal{D}$ for inclusive two-jet events at parton level and after the loose set of selection cuts. The result for exclusive three-jet events is shown in Table V. As explained above, the degree of polarization is the same in the helicity basis using the tq-frame and the spectator basis as a result of the event kinematics. This is true even after reconstruction. The top quark is almost completely polarized in the helicity and spectator bases, and the $O(\alpha_s)$ corrections only degrade that picture slightly. At the parton level, the degree of top quark polarization in the helicity basis is larger in the tq-frame than in the $tq(j)$-frame. After event reconstruction there is a dependence on the selection cuts. For the loose selection cuts, the tq-frame is better than the $tq(j)$-frame, whereas for the tight selection cuts the $tq(j)$-frame is better. The tight selection cuts require a forward untagged jet and a central, large b-tagged jet p_T, thus modifying the event kinematics, supressing the HEAVY correction and enhancing the LIGHT corrections, see Figs. 12 and 10. As a result the degree of polarization in the $tq(j)$-frame is increased. The beamline basis produces only small degrees of polarization as expected. This gets better when choosing a direction in the η beamline basis. Especially for tight cuts which require the spectator jet to be forward, the polarization in the η beamline basis improves, but even then it is still smaller than in the helicity or spectator basis. $\mathcal{D}$ is also consistently smaller for antitop quarks than for top quarks for all methods. In the exclusive three-jet sample, the degree of polarization is further reduced because the third jet affects the kinematics of either the spectator jet or the top quark. The spin polarization measurements at higher CM energies show the same result.

Our study shows that the helicity basis (using the tq-frame) and the spectator basis are equally good to study the top quark polarization. In the s-channel process, the measured polarization could be enhanced significantly by choosing a direction for the incoming down-type quark based on the boost of the virtual W boson [36]. In the t-channel this is also useful for the beamline basis. However, even after such a choice that basis still produces a smaller degree of polarization than the helicity or spectator bases.

	Top		Antitop	
	LO	NLO	LO	NLO
Helicity basis:				
Parton level (tq-frame)	0.99	0.91	0.93	0.86
Parton level ($tq(j)$-frame)		0.66		0.62
Loose selection (tq-frame)	0.70	0.60	0.63	0.56
Loose selection ($tq(j)$-frame)		0.58		0.54
Tight selection (tq-frame)	0.71	0.72	0.69	0.73
Tight selection (($tq(j)$-frame)		0.76		0.76
Spectator basis:				
Parton level	-0.99	-0.91	0.93	0.86
Reconstructed events	-0.70	-0.60	0.63	0.56
Beamline basis:				
Parton level	-0.20	-0.15	0.14	0.11
Loose selection	-0.14	-0.09	0.07	0.06
Tight selection	-0.28	-0.26	-0.20	-0.21
η beamline basis:				
Parton level	-0.64	-0.64	-0.77	-0.67
Loose selection	-0.56	-0.49	-0.62	-0.49
Tight selection	-0.61	-0.50	-0.63	-0.53
$\hat{s}$ beamline basis:				
Loose selection	-0.41	-0.26	-0.38	-0.14

TABLE IV: Degree of polarization $\mathcal{D}$ for inclusive two-jet single top quark events, at parton level before cuts and after selection cuts in the t-channel process at the 7 TeV LHC. The $tq(j)$-frame in the helicity basis denotes the c.m. frame of the incoming partons, while the tq-frame denotes the rest frame of the top quark and spectator jet.

V. CONCLUSIONS

We have presented a next-to-leading order study of t-channel single top and antitop quark production at the LHC proton-proton collider for several CM energies, including $O(\alpha_s)$ QCD

	Top	Antitop
Helicity basis:		
Loose cuts (tq-frame)	0.60	0.53
Loose cuts ($tq(j)$-frame)	0.58	0.50
Tight cuts (tq-frame)	0.67	0.66
Tight cuts ($tq(j)$-frame)	0.73	0.71
Spectator basis:		
Loose cuts	-0.60	-0.53
Beamline basis:		
Loose cuts	-0.14	-0.08
Tight cuts	-0.28	-0.35
η beamline basis:		
Loose cuts	-0.47	-0.48
Tight cuts	-0.60	-0.59
$\hat{s}$ beamline basis:		
Loose cuts	-0.29	-0.22

TABLE V: Degree of polarization $\mathcal{D}$ at for exclusive three-jet t-channel events after selection cuts at the 7 TeV LHC. The $tq(j)$-frame in the helicity basis denotes the c.m. frame of the incoming partons, while the tq-frame denotes the rest frame of the top quark and spectator jet.

corrections to both the production and decay of the top quark. The $O(\alpha_s)$ corrections affect top and antitop quark production differently and also show a dependence on the CM energy. The inclusive t-channel cross section for the production of a single top (antitop) quark with a mass of 173 GeV at 7 TeV is 40.0 ± 4.6 pb (21.9 ± 4.1 pb), where the uncertainty includes scale, top quark mass, and PDF components. For top quark production this is only an increase of 4% compared to Born-level. For antitop quark production the increase compared to Born-level is larger at 15%. The behavior is similar for higher collider CM energies. The impact of kinematical cuts on the acceptances has been studied for a loose and a tight set of cuts, corresponding to typical event selections used by the ATLAS and CMS collaborations at the LHC. We find that the acceptances are sensitive to the $\Delta R_{\rm cut}$ we imposed on the jet cone size and the lepton isolation. With the choice of $\Delta R_{\rm cut} = 0.4$, the difference between

the Born-level and NLO acceptances is about 5% for a loose cut set and slightly larger when changing $\Delta R_{\rm cut}$ from 0.4 to 0.5. For antitop quark production the difference between the Born-level and NLO acceptances is about 15%, and again slightly larger when increasing $\Delta R_{\rm cut}$ from 0.4 to 0.5.

We have categorized the $O(\alpha_s)$ contributions to the t-channel single top process into three gauge invariant sets: the light quark line corrections, the heavy quark line corrections and the top quark decay corrections. This allows us to analyze the $O(\alpha_s)$ corrections in detail and facilitates comparisons with event generators. The corrections affect the shape of some of the important kinematic distributions and result in a large fraction of events containing three reconstructed jets in the final state for the loose set of kinematic cuts. The acceptance for t-channel single top quark events and the fraction of 3-jet events depend strongly on the jet p_T cut. The kinematic distributions affected by the radiative corrections include those that separate the t-channel single top signal from the various backgrounds, such as the pseudo-rapidity distribution of the spectator jet. We find that the $O(\alpha_s)$ LIGHT and HEAVY corrections have almost opposite effects on various pseudo-rapidity distributions, due to the difference in the parton distribution functions between the valence quarks and sea quarks. The former shifts the spectator jet to even higher pseudo-rapidities, while the later shifts it to more central pseudo-rapidity regions. The summed contributions cause the spectator jet to be even more forward which will change the prediction of the acceptance for t-channel single top quark events. Also, a large fraction of three jet events contain two b-jets due to the collinear enhancement in the $W + g$ fusion process. This also impacts the experimental choice of the light quark jet in 3-jet events. Choosing the most forward jet (highest $|\eta|$) is correct in only 80% of the events, while choosing the highest p_T jet is correct in over 90% of the events.

In order to study top quark properties such as the top quark polarization, induced from the effective t-b-W couplings, we reconstruct the top quark by combining the W boson with the leading b-tagged jet. We use the top quark thusly reconstructed to explore spin correlations in three different bases: the helicity basis, the spectator basis and the beamline basis. The degree of polarization is very large in the helicity and spectator bases. Its reduced after event reconstruction, especially for antitop quark production. The radiative corrections reduce the degree of polarization further, both at parton level and after event reconstruction.

Acknowledgments

S. H. and R. S. are supported in part by the U.S. National Science Foundation under Grant No. PHY-0757741. Q. H. C. is supported in part by the Argonne National Laboratory and University of Chicago Joint Theory Institute (JTI) Grant No. 03921-07-137, and by the U.S. Department of Energy under Grants No. DE-AC02-06CH11357 and No. DE-FG02-90ER40560. C. P. Y. acknowledges the support of the U.S. National Science Foundation under Grants No. PHY-0555545 and PHY-0855561. Q.H.C thanks Shanghai Jiaotong University for hospitality where part of this work was done. C. P. Y. would also like to thank the hospitality of National Center for Theoretical Sciences in Taiwan and Center for High Energy Physics, Peking University, in China, where part of this work was done.

---

[1] C.-R. Chen, F. Larios, and C. P. Yuan, Phys. Lett. **B631**, 126 (2005), hep-ph/0503040.

[2] V. M. Abazov et al. (DØ collaboration), Phys. Rev. Lett. **101**, 221801 (2008), arXiv:0807.1692 [hep-ex].

[3] V. M. Abazov et al. (DØ collaboration), Phys. Rev. Lett. **102**, 092002 (2009), arXiv:0901.0151 [hep-ex].

[4] V. M. Abazov et al. (DØ collaboration), Phys. Rev. Lett. **103**, 092001 (2009), arXiv:0903.0850 [hep-ex].

[5] T. Aaltonen et al. (CDF collaboration), Phys. Rev. Lett. **103**, 092002 (2009), arXiv:0903.0885 [hep-ex].

[6] Tevatron Electroweak Working Group (CDF collaboration and DØ collaboration) (2009), arXiv:0908.2171 [hep-ex].

[7] V. M. Abazov et al. (DØ collaboration), Phys. Rev. Lett. **98**, 181802 (2007), hep-ex/0612052.

[8] V. M. Abazov et al. (DØ collaboration), Phys. Rev. **D78**, 012005 (2008), arXiv:0803.0739 [hep-ex].

[9] T. Aaltonen et al. (CDF collaboration), Phys. Rev. Lett. **101**, 252001 (2008), arXiv:0809.2581 [hep-ex].

[10] V. M. Abazov et al. (DØ collaboration), Phys. Lett. **B682**, 363 (2010), arXiv:0907.4259 [hep-ex].

[11] V. M. Abazov et al. (DØ collaboration), Phys. Rev. **D75**, 092007 (2007), hep-ex/0604020.

[12] T. Aaltonen et al. (CDF collaboration), Phys. Rev. **D82**, 112005 (2010), arXiv:1004.1181 [hep-ex].

[13] T. M. P. Tait and C.-P. Yuan, Phys. Rev. **D63**, 014018 (2000), hep-ph/0007298.

[14] Q.-H. Cao, J. Wudka, and C.-P. Yuan, Phys.Lett. **B658**, 50 (2007), arXiv:0704.2809 [hep-ph].

[15] J. Aguilar-Saavedra, Nucl.Phys. **B843**, 638 (2011), arXiv:1008.3562 [hep-ph].

[16] C. Zhang and S. S. Willenbrock (2010), arXiv:1008.3869 [hep-ph].

[17] M. C. Smith and S. S. Willenbrock, Phys. Rev. **D54**, 6696 (1996), hep-ph/9604223.

[18] G. Bordes and B. van Eijk, Nucl. Phys. **B435**, 23 (1995).

[19] B. W. Harris, E. Laenen, L. Phaf, Z. Sullivan, and S. Weinzierl, Phys. Rev. **D66**, 054024 (2002), hep-ph/0207055.

[20] Z. Sullivan, Phys. Rev. **D70**, 114012 (2004), hep-ph/0408049.

[21] J. Campbell, R. K. Ellis, and F. Tramontano, Phys. Rev. **D70**, 094012 (2004), hep-ph/0408158.

[22] Q.-H. Cao and C. P. Yuan, Phys. Rev. **D71**, 054022 (2005), hep-ph/0408180.

[23] Q.-H. Cao, R. Schwienhorst, and C. P. Yuan, Phys. Rev. **D71**, 054023 (2005), hep-ph/0409040.

[24] Q.-H. Cao, R. Schwienhorst, J. A. Benitez, R. Brock, and C. P. Yuan, Phys. Rev. **D72**, 094027 (2005), hep-ph/0504230.

[25] S. Frixione, E. Laenen, P. Motylinski, B. R. Webber, and C. D. White, JHEP **0807**, 029 (2008), arXiv:0805.3067 [hep-ph].

[26] S. Alioli, P. Nason, C. Oleari, and E. Re, JHEP **0909**, 111 (2009), arXiv:0907.4076 [hep-ph].

[27] E. Re (2010), arXiv:1009.2450 [hep-ph].

[28] P. Falgari, P. Mellor, and A. Signer, Phys. Rev. **D82**, 054028 (2010), arXiv:1007.0893 [hep-ph].

[29] J.M. Campbell, R. Frederix, F. Maltoni, and F. Tramontano, Phys. Rev. Lett. **102**, 182003 (2009), arXiv:0903.0005 [hep-ph].

[30] J. M. Campbell, R. Frederix, F. Maltoni and F. Tramontano, JHEP **0910**, 042 (2009) arXiv:0907.3933 [hep-ph].

[31] N. Kidonakis, Phys. Rev. **D75**, 071501 (2007), hep-ph/0701080.

[32] N. Kidonakis, Phys.Rev. **D81**, 054028 (2010), arXiv:1001.5034 [hep-ph].

[33] N. Kidonakis, Phys. Rev. D **74**, 114012 (2006) hep-ph/0609287.

[34] H. X. Zhu, C. S. Li, J. Wang, and J. J. Zhang (2010), arXiv:1006.0681 [hep-ph].

[35] J. Wang, C. S. Li, H. X. Zhu, and J. J. Zhang (2010), arXiv:1010.4509 [hep-ph].

[36] S. Heim, Q.-H. Cao, R. Schwienhorst, and C. P. Yuan, Phys. Rev. **D81**, 034005 (2010), arXiv:0911.0620 [hep-ph].

[37] J. Pumplin et al. (CTEQ collaboration), JHEP **07**, 012 (2002), hep-ph/0201195.

[38] P. M. Nadolsky et al. (CTEQ collaboration), Phys. Rev. **D78**, 013004 (2008), arXiv:0802.0007 [hep-ph].

[39] Q.-H. Cao and C.-P. Yuan, Phys. Rev. Lett. **93**, 042001 (2004), hep-ph/0401026.

[40] V. M. Abazov et al. (DØ collaboration), Phys. Rev. Lett. **101**, 182001 (2008), arXiv:0807.2141 [hep-ex].

[41] T. Aaltonen et al. (CDF collaboration), Phys. Rev. **D79**, 092005 (2009), arXiv:0809.4808 [hep-ex].

[42] Tevatron Electroweak Working Group (CDF collaboration and DØ collaboration) (2010), arXiv:1007.3178 [hep-ex].

[43] W. T. Giele and E. W. N. Glover, Phys. Rev. **D46**, 1980 (1992).

[44] W. T. Giele, E. W. N. Glover, and D. A. Kosower, Nucl. Phys. **B403**, 633 (1993), hep-ph/9302225.

[45] J. M. Campbell and F. Tramontano, Nucl. Phys. B **726**, 109 (2005) hep-ph/0506289.

[46] C. E. Gerber et al. (The TeV4LHC Top and Electroweak Working Group) (2007), arXiv:0705.3251 [hep-ph].

[47] B. Clement et al. (ATLAS collaboration) (2009), aTL-PHYS-PUB-2009-042.

[48] C.-P. Yuan, Phys. Rev. **D41**, 42 (1990).

[49] J. Alitti et al. (UA2 collaboration), Phys. Lett. **B257**, 232 (1991).

[50] G. Aad et al. (ATLAS collaboration) (2009), arXiv:0901.0512 [hep-ex].

[51] G. L. Bayatian et al. (CMS collaboration), Journal of Physics G: Nuclear and Particle Physics **34**, 995 (2007), URL `http://stacks.iop.org/0954-3899/34/995`.

[52] P. Motylinski, Phys. Rev. **D80**, 074015 (2009), arXiv:0905.4754 [hep-ph].

[53] G. Mahlon and S. J. Parke, Phys. Rev. **D53**, 4886 (1996), hep-ph/9512264.

[54] G. Mahlon and S. J. Parke, Phys. Lett. **B476**, 323 (2000), hep-ph/9912458.

[55] G. Mahlon (1998), hep-ph/9811219.